

MECHANICAL PROPERTIES AND CRACKING POTENTIAL OF ALKALI-
ACTIVATED MATERIALS CONTAINING WASTE GLASS POWDER

by

Mehrab Nodehi, B.S.

A thesis submitted to the Graduate Council of
Texas State University in partial fulfillment
of the requirements for the degree of
Master of Science
with a Major in Engineering
May 2022

Committee Members:

Xijun Shi, Chair

Togay Ozbakkaloglu, Co-Chair

Federico Aguayo

COPYRIGHT

by

Mehrab Nodehi

2022

FAIR USE AND AUTHOR'S PERMISSION STATEMENT

Fair Use

This work is protected by the Copyright Laws of the United States (Public Law 94-553, section 107). Consistent with fair use as defined in the Copyright Laws, brief quotations from this material are allowed with proper acknowledgement. Use of this material for financial gain without the author's express written permission is not allowed.

Duplication Permission

As the copyright holder of this work I, Mehrab Nodehi, authorize duplication of this work, in whole or in part, for educational or scholarly purposes only.

ACKNOWLEDGEMENTS

I would like to thank Texas State University and the Lone Star State for allowing and supporting me to reach this level of academic standing.

I would like to express my sincere gratitude to my advisor and committee members, Dr. Xijun Shi, Dr. Togay Ozbakkaloglu and Dr. Federico Aguayo, for their great support and patience that helped me throughout this research process. Also, specific thanks to Dr. Vishu Viswanathan for if it had not been for his support, I would have never been able to conduct this research. Lastly, I would like to thank the faculty and staff of the Ingram School of Engineering, especially Dr. Ravi Droopad, for their continuous support throughout this research.

TABLE OF CONTENTS

	Page
ACKNOWLEDGEMENT	iv
LIST OF TABLES	vi
LIST OF FIGURES	vii
LIST OF ABBREVIATIONS	viii
ABSTRACT	ix
CHAPTER	
1. INTRODUCTION	1
2. LITERATURE RIVIEW.....	4
3. MIXTURE AND MATERIALS	14
4. TEST RESULTS AND DISCUSSION.....	28
5. CONCLUSION	53
REFERENCES	56

LIST OF TABLES

Table	Page
1. The potential production and estimated consumption of selected materials with pozzolanic ability (mt/y: million metric ton) [22], [24].....	2
2. Common glass powder sizes used in literature and their respective findings.....	6
3. A brief overview of AAMs [63], [64].....	7
4. Brief review of common supplementary cementitious materials with uses as aluminosilicate sources (or precursor) for AAMs	8
5. Major activators used in literature with a brief description.....	10
6. Physico-chemical properties of Portland cement used in this study.....	14
7. Physical properties of aggregates used in this study, based on ASTM C128	15
8. Physico-chemical properties of the coal fly ash and GGBFS used in this study	16
9. Physico-chemical properties of glass powder	16
10. Mixture proportions	18
11. Experiments conducted in this research along with other details	19
12. Information about restrained shrinkage specimens.....	47
13. Presenting the area and radius of colonies of unreacted particles found in surface morphology test	52

LIST OF FIGURES

Figure	Page
1. Sieve analysis of aggregates conducted based on ASTM C 136 [1]	15
2. The test set up of restrained shrinkage fixtures.....	26
3. Flowability of mixes	29
4. Air content of mixes.....	30
5. Fresh and hardened density of mixes.....	31
6. Compressive strength of mixes	33
7. Splitting tensile strength of mixes.....	34
8. The result of (a) elastic modulus, (b) and (c) comp. strength to elastic modulus.....	35
9. Abrasion resistance of mixes.....	37
10. The result of (a) water absorption and (b) apparent porosity of mixes	39
11. The result of (a) autogenous shrinkage, (b) drying shrinkage and (c) mass loss of mixes exposed to drying shrinkage condition.....	41
12. The recorded micro strain values of various mixes	43
13. Cracks formed on top of the specimens.....	45
14. Cracks formed on sides of the specimens with (a): GEFA50GP50, (b): GEFA0GP50, (c): PCFA25GP0, (d): PCFA0GP25.....	46
15. Graphical illustration of the observed cracks.....	47
16. Electrical resistivity of mixes	48
17. Digital images of mixes with size designation of the un-hydrated particles showing length, radius, diameter and area	50

LIST OF ABBREVIATIONS

Abbreviation	Description
AAMs	Alkali-activated materials
OPC	Ordinary portland cement
w/c	water-cement ratio
MSWI ash	Municipal solid waste incinerated ash
C&D	Construction and demolition
LCA	Life cycle assessment
NaOH	Sodium hydroxide
KOH	Potassium hydroxide
Na ₂ SO ₄	Sodium sulfate
K ₂ CO ₃	Potassium carbonate
GGBFS	Ground granulated blast furnace slag
ASTM	American Society for Testing and Materials

ABSTRACT

In the construction industry, the production, processing, and transportation of ordinary portland cement (OPC) is a significant contributor of greenhouse gas emissions that can lead to environmental degradation and even resource depletion. To mitigate the negative impacts of OPC and improve concrete performance, supplementary cementitious materials (SCMs) have been used for decades. However, the projected reduction in the availability of traditional SCMs, such as coal fly ash has increased the interest in searching for alternative and widely available SCMs. One of such materials is glass that has an annual production around 100 million tons, but due to the high energy consumption in recycling glass, the glass industry has a low recycling rate (about 26%). The use of ground waste glass as a SCM can have substantial energy and economic implications due to the reduction in landfilling of this waste material. In this study, the mechanical properties and cracking potential of traditional portland cement based- and alkali-activated materials containing waste glass powder via a series of mechanical tests and a customized ring test. The results showed that the aluminosilicate-based glass powder performs very differently in each binding system, possibly because of its Al content contributing to geopolymerization in geopolymer mortars. Further, the result of restrained shrinkage test showed that the cracking duration, style and width are significantly different in each binding system. The result of this study is significant and point to different performance of glass powder in portland cement and geopolymer binders.

1. INTRODUCTION

The increase in use of energy since the industrial revolution has been a steady trend that continues to this date. This steadfast increase comes in the form of heavy production, usage and generated waste byproducts. Within the construction industry, the production of OPC is linked with calcination process that occurs at high temperatures that accounts for almost 8% of total global CO₂ production [2], [3]. As a result, to promote efficiency and sustainability in the construction industry, a great deal of research has been conducted on the use of sustainable materials in concrete in the last few decades. As of 2019, the top OPC producing countries are reported to be: China with 2,200, India with 320, and United States with 89, million metric tons, annually [4]. This vast production is directly linked with almost more than 7.5 million and 12.7 million employment in the U.S. and Europe, respectively [5], [6]. While countries are outpacing each other in OPC production, modernization and vast urbanization, it is important to follow efficient means for sustainable development [7]–[10]. Currently, there are two common trends of minimizing the greenhouse effects in the construction industry. With the first focusing on the concept of green and sustainable buildings mainly in their energy efficiency, and the other focusing on the production of greener and recycled materials by looking at their whole life cycle. This is done through the frequently used life cycle assessment (LCA) tool as a means to evaluate the environmental impact of a product [11]. LCA, in that respect, provides environmental impact analysis of the material's life cycle, which, according to previous studies, has showed the potential of reusing recycled materials in lowering the environmental impact of concrete [3], [12]–[22]. The most common and favorable waste materials that have been used to reduce the environmental impact of

concrete include SCMs and construction waste and demolition (C&D). In particular, the use of SCMs in concrete production can have a much more significant sustainability effect due to replacing OPC with green and alternative materials.

Previous studies, for instance, have reported that SCMs processing has a smaller CO₂ emission contribution and is approximated to have an overall energy consumption of around 8.6 MJ/m³ as opposed to 790 MJ/m³ compared to OPC [23]. Yet, over time, the commonly used SCMs have found a variety of applications to the point that their values have risen to be comparable, or even somewhat higher than OPC, in some cases (e.g., silica fume). In the same way, the most commonly used SCM, coal fly ash, is projected to have a significant reduction in its production rate due to the environmental concern of coal burning in electricity generation sector [24]. As a result, the quest for alternative eco-friendly SCMs has prompted major research efforts to find other suitable materials for OPC substitution. To secure such promising materials, recent studies have shown the possibility of using glass powder as a cementitious material that can have a comparable reaction rate of coal fly ash [21]. Table 1 further elaborates on the estimated production and consumption of commonly used SCMs with selected alternatives that also have cementitious or pozzolanic properties.

Table 1. The potential production and estimated consumption of selected materials with pozzolanic ability (mt/y: million metric ton) [22], [24].

Material	Major compositions	Production (Mt/y)	Estimated consumption (Mt/y)
Silica Fume	Si	1-2.5	70-90%
Ground Granulated Blast Furnace Slag (GGBFS)	Ca-Si-Al	300-360	70-90%
Fly Ash	Si-Al and Si-Ca-Al	900	58-64%
Glass	Si-Al-Ca	100	26%
Metakaolin	Si-Al	2.2-2.6	N/A
Rice husk ash	Si-C-K ₂ O	30	negligible
MSWI ash	Si-Al-Ca	30-60	negligible
Red mud	Fe-Al-Si	140	2-4

1.1. Research gap

To mitigate the high greenhouse gas generation, as a result of OPC production, most commonly, various types of SCMs ranging from natural pozzolans, industrial byproducts, and even agricultural waste, have been used. Yet, since one of the most favorable and commonly used SCMs, coal fly ash, is projected to have a major production reduction, this research proposes utilizing waste glass powder since glass has a considerable availability on a global scale with a relatively high production rate and a low recycling rate, due to the costs associated with its recycling process. In addition, since glass is basically a ceramic, it has a good compatibility with conventional and geopolymer concrete and can potentially result in better thermo-mechanical and thermo-durability properties. As a case in point, considering the high hardness and melting point of glass, it can be used in major infrastructure that require high abrasion resistance and thermal properties. As a result, this research proposes utilizing recycled glass powder in two commonly researched binding agents of AAMs (or geopolymer) system, as well as conventional portland cement mortar.

2. LITERATURE REVIEW¹

In this chapter, current progress in commonly used SCMs in ordinary concrete and AAMs area, as well as commonly used activators for AAMs are reviewed and discussed. By reviewing different types of waste materials that have been utilized in conventional concrete and AAMs, the author intends to propose new work that will fill the knowledge gaps of the previous research.

2.1. SCMs and ground glass

Starting from the mid-1940s, studies conducted by Purdon and Glukhovsky [25] on industrial wastes such as ground granulated blast furnace slag (GGBFS) and later on coal fly ash [26] showed sustainability benefits and cost reduction by incorporating such waste-based materials to in concrete. Through the inclusion of such SCMs, an overall greenhouse gas emission reduction of up to 22-37% was reported to be achieved [27], [28]. Recently, as a result of environmental protection laws, as well as the change in the form of energy production from coal to renewable energies, the production of one of the major SCMs, coal fly ash, that had seen up to 900 million tons of annual production [29], [30], started to decline and is projected to experience a steady 10-20% production reduction annually [31], [32]. Thus, the interest for finding other waste materials that can replace coal fly ash in concrete has grown rapidly. In this environment, among the most commonly available materials, waste glass has recently been found to have a pozzolanic behavior which is comparable to coal fly ash. Considered as one of the most available solid waste materials, waste glass is an amorphous, non-crystalline material that has a high content of silicon (Si) [33], [34]. Waste glass is estimated to have an annual

¹ Parts of this chapter are reprinted from authors' previous work available at [21], [24]

production of around 100 million tons, but only around 26% has been reported to be recycled [35]. The glass industry is recognized as an energy intensive industry with an estimated 16.9 MJ of energy being consumed and 0.57 kg of CO₂ being produced per 1 kg of glass sheet [36]. Although glass may be endlessly recycled [37], the current high cost and energy consumption associated with the recycling procedure makes it more cost-effective to landfill waste glass [38], [39].

Glass has the potential to be used not only as a SCM but also as a fine aggregate [40]–[43], but also be used as fine sand [44], [45]. Currently, glass is mainly manufactured with three main types: borosilicate, aluminosilicate, and soda-lime based glass [46]. In general, the most available glass material considered as solid waste is the soda-lime-based glass [46] that consists of more than 70% silica [47]. It can dissolve in the highly alkaline medium of the mixture and participate in the hydration process of OPC, reacting with calcium hydroxide and producing calcium silicate hydrate (C-S-H) [40]. However, for waste glass to be used as an ingredient of construction materials, grinding and crushing [48] procedures may be needed, and the procedures can lead to environmental and technical impacts that should further be assessed. Nonetheless, the mentioned paradigm shift in the availability of SCMs prompted researchers to utilize glass powder with the main focus on its potential in substituting OPC in concrete. Table 2 shows some of the recently published research articles that have used glass as SCM.

Table 2. Common glass powder sizes used in literature and their respective findings

Type of glass	Glass powder size	Max inclusion (%)	Comments	Reference
Soda lime glass bottles	3.4 μm	30	High resistance to Chloride ion and water penetration have been reported.	[49]
Waste glass and waste glass sludge	14.7 μm	20	Better performance of finer particles, better freeze thaw, and RCPT, results in either form, reported.	[50]
Unspecified	<100 μm	20	Lower reduction in ASR compared to coal Fly ash, better permeability resistance compared to OPC and reduced total moisture intake.	[51]
Waste glass bottles	90 μm	30	Better sulfate and acid resistance, and lower permeability was achieved.	[52]
Crushed waste glass	<75 μm	30	Increase in workability, reduction in density due to free water, low porosity and lower permeability.	[53]
Soda-lime glass	<150 μm	60	Noted the consumption of CH through pozzolanic reaction after a year of curing, higher porosity of high volume OPC replacement where better resistance to transport of water and chloride ions attributed to densified ITZ.	[54]
Unspecified	<75 μm	25	Increase in slump, based on TGA results, glass powder satisfies the limits of coal fly ash according to ASTM C618, highlighting that W/C reduction of mixture as a result of better workability, can mitigate the strength reduction.	[55]
Calcium aluminosilicate, soda-lime and silica glass	~10 μm	20	Enhanced early hydration due to finer powder size, higher hydration rate of calcium-aluminosilicate based glass powder, significant improvement in electrical resistivity that is noted to be much higher than that of coal fly ash.	[56]
Clear and green glass	25 μm	25	Effect of curing temperature noted as a direct effect on pozzolanic behavior	[57]

2.2. Alkali-activated materials²

AAMs are an alternative binding system that consists of a high volume of waste materials (e.g., coal fly ash and GGBFS). Since their recognition and discovery by Purdon [25] and Glukhovsky during the 1940s and 1950s, numerous studies were dedicated to their use in different applications, such as eco-friendly concrete [58], [59], ceramic formation [60], [61] and refractories [62]. Unlike portland cement that reacts

² Although in definition the term AAMs refers to a more comprehensive group of materials than the term geopolymers, the two terms are mostly used interchangeably in literature. As a result, in this work the term AAMs is used throughout the text.

with water, AAMs require an alkaline activator to increase the reactivity of the aluminosilicate-bearing materials (also referred as precursor), releasing Si, Ca, Al and other minerals needed for reformation and creation of the binder. In that respect, liquid and solid activators (generally sodium silicate, sodium hydroxide and sodium metasilicate) are commonly used to increase the pH of the medium and activate the precursors' ability to glue the mixture together [24]. Based on the type of precursor and activator, AAMs are divided into: 1. Low calcium, 2. High calcium, and 3. Hybrid systems. Table 3 provides a brief description of the terms associated AAMs.

Table 3. A brief overview of AAMs [63], [64].

Alkali-activated materials systems	Description
Low calcium binders	The low calcium system refers to the mixtures that the calcium content in the aluminosilicate source is relatively low (generally coal fly ash class F based geopolymer). In such system, most often thermal curing is required, in addition to the activator to increase the strength gain rate. This type of AAMs is also called geopolymer and has been initially used mainly with Metakaolin precursor to reduce the need for thermal curing.
High calcium binders	In high calcium system the major aluminosilicate source is often FA (class C) or GGBFS whereby due to the higher content of calcium the strength development is relatively higher and no specific curing regime is required.
Hybrid (blended alkali) systems	In systems where the combination of high calcium and low calcium precursors, often with OPC, is used which allows different low reactivity precursors to be used without specific curing.
Performing type	Description
Two-part	The activation process generally takes place with the addition of a liquid activator such as sodium silicate. In such applications where the activator is in a liquid state and is added to start the strength gain, the procedure is referred to as two-art AAMs.
One-part	In applications where a solid activator such as sodium metasilicate anhydrous are used, the procedure is referred to as one-part AAMs.

2.2.1. Precursors In AAMs are aluminosilicate-bearing raw materials that dissolve by the activators. These materials include coal fly ash [65], [66], GGBFS [67], [68], metakaolin [69], rice husk ash [70], red mud [71], [72], and other reactive materials that are rich in silica (SiO₂) and alumina (Al₂O₃) [73] [74]. Table 4 provides a brief description of the most commonly used precursors for the production of AAMs. In AAMs, precursors provide a range of dissolved and reactive elemental materials that rearrange to harden, and the variation in aluminum, calcium, and silicate contents of these precursors are major factors affecting the resulting concrete materials.

Table 4. Brief review of common supplementary cementitious materials with uses as aluminosilicate sources (or precursor) for AAMs.

Name of the SCM	Description
Fly ash	Divides into class F and C, with class C having a higher calcium content and being more reactive with a rather variable composition. In general, Fly ash is one of the most commonly used SCM but is projected to experience an annual decrease of 11-20% until 2050 due to reduced coal use, according to EPA [31], [76]. The inclusion of Fly ash results in better rheology and durability while increasing the initial setting time [77]–[79].
Ground Granulated blast furnace slag (GGBFS)	GGBFS is the 2 nd commonly used SCM which is a byproduct of pig iron production process. Due to its major similarity in cementitious properties, it is already being used in high quantities in OPC production.
Metakaolin	Metakaolin is the byproduct of porcelain production and its major use has been in low-calcium AAMs where it increases the reactivity to the point that no thermal curing is required. Compared to OPC, it has smaller sizes of around 1 to 20 μm and is reported to enhance the interfacial transition zone [80]–[84].
MSW ash	MSW incineration ash has a production of over 30 Mt/y ³ that is reported to have cementitious properties. It can be used in cement production of substitute some amount of OPC providing more compaction to the final product [85].
Biomass ash	Biomass ash refers to the mass of burnt organic matter and is a source of silica (Si) that has been reported to be beneficial in increasing the compaction while added up to 25 binder w% [86], [87].
Paper sludge	Paper sludge refers to the micro-fibers produced as a result of paper production process. Its use in concrete mixture is reported to reduce the drying shrinkage and reduce flowability. Paper sludge is a rich source of Fe and Si. [91], [92]
Mine tailings	Through the process of mining a large content of materials are often moved and dumped. Such materials have a variable property according to their composition and include coal refuse (coal tailings), phosphate tailings and Bauxite tailings (generated as a result of aluminum mining and is also called red mud) [93], [94].

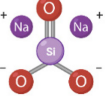
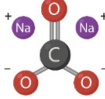
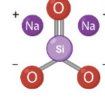
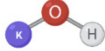
³ Million metric tons / year

2.2.1.1. The use of glass powder as a precursor Waste glass powder has recently been practiced to substitute precursor in AAMs and has been found to have acceptable pozzolanic properties [95], [96]. This property is known to be due to its chemical composition containing of SiO_2 , Al_2O_3 , and CaO that can directly take part in geo-polymerization process [95]. Yet, the reactivity degree of glass powder is reported to have a direct relationship with its particle size. According to previous (as in [97], [98]) studies, a fine glass powder size of around 30-100 μm can have a reaction rate comparable to class F coal fly ash.

2.2.2. Activators Alkali-activation is a complex and multi-chain function that takes place in alkaline solution where the aluminosilicate materials dissolve to form a new network structure. This process starts by ion exchange and hydrolysis of Si and Al followed by their network breakdown. The alkaline solution has two basic roles in the AAMs mixture: (1) Dissolving Si-O and Al-O bonding and facilitating their subsequent re-establishment in the AAMs network, and (2) Charge-balancing of the mixture by alkali-metal cations [99]. In short, Alkali-activator acts as a catalyst in the reaction, allowing the new and polymeric formation. Pimraksa et al. [100], for instance, showed that the higher molar ratios of $\text{SiO}_2/\text{Al}_2\text{O}_3$ and $\text{Na}_2\text{O}/\text{Al}_2\text{O}_3$ lead to higher mechanical strength and density of the resulting AAMs. For activators, sodium hydroxide (NaOH) was proved to perform better than potassium hydroxide (KOH) in their study. Sodium hydroxide (NaOH), potassium hydroxide (KOH), sodium sulfate (Na_2SO_4), and potassium carbonate (K_2CO_3) are major activators utilized in liquid form, while sodium metasilicate (Na_2SiO_3), sodium carbonate (Na_2CO_3), and potassium hydroxide

(KOH) are the major activators used in solid form. The sodium-based alkali-activators are generally more available at lower costs with high reactivity, while potassium-based activators have been widely entertained for high temperature applications [101]. Table 5 further reviews the mentioned activators.

Table 5. Major activators used in literature with a brief description.

Name	Common State Used	Description and Comments	Chemical Structure
Sodium hydroxide	Liquid	Sodium hydroxide (<i>NaOH</i>), also known as <i>caustic soda</i> , is an inorganic compound that has a variety of uses in manufacturing processes including soaps, paper, dye, and petroleum products. Since it is a <i>strong base</i> , it has a corrosive nature and can cause allergic reactions and skin irritations [102]. It can be found in liquid and solid states that are both colorless and have no odor.	
Sodium silicate	Liquid	Sodium silicate is a general name of any chemical compound that has sodium oxide, $(\text{Na}_2\text{O})_n$, and silica $(\text{SiO}_2)_m$, in it. It has a variety of applications in construction industry that includes sealing of concrete cracks, and dissolving the precursor in AAMs, and setting accelerator [103]. The commercially available Sodium silicate has a pH of around 10 to 13, inversely relating to the silica content.	
Sodium carbonate	Solid	Sodium carbonate is another inorganic compound that is water-soluble. With formula Na_2CO_3 , it has a high concentration of bicarbonate that increases pH or leads to dissolution of other matters within the medium [104]. This solid material can be produced from natural sources of trona and sodium carbonate brines, as well as nahcolite mineral (naturally occurring sodium bicarbonate) sources [105] which commonly occurs as crystalline decahydrate that subsequently effloresces and forms an odorless and white powder [106].	
Sodium metasilicate	Solid	Sodium metasilicate is the main component of sodium silicate with Na_2SiO_3 formula. The production of Sodium metasilicate is an energy-intensive process that requires the fusion of silica sand (SiO_2) with sodium carbonate (soda ash) that occurs at around 1400°C [107].	
Potassium hydroxide	Solid	With formula <i>KOH</i> , potassium hydroxide is a strong base that is commercialized in pellets, flakes and powder that is known for its corrosiveness tendency to absorb moisture from the environment. The production of potassium hydroxide is done through electrolysis of potassium chloride. Severe reactions, skin irritations and other hazardous side effects have been documented as a result of contact with it [108]	

2.2.3. Alkali-concentration of activators An aqueous solution comprises of solvent and solute, and the alkali-concentration is a measure of the dissolved moles in the solution. This, in other words, translates into the moles of the solute expressed by the volume liters as written in Eq. 1:

$$\text{Molarity (M)} = \frac{\text{The number of moles of solute (n)}}{\text{Volume of the solution (v)}} = \frac{\text{Mol}}{\text{Liter}} \quad \text{Eq. 1}$$

In AAMs, the molarity, or concentration of the activator, has been proven to be a critical factor in the hydrolysis of the aluminosilicate materials [109]. In lower concentrations, insufficient dissolution of the precursors as well as lower polymerization is reported [110]. This, however, does not mean that the higher the activator concentration, the better the AAMs are. As discussed in detail by Xu et. al. and Hounsi et. al. [111], [112], unconditionally high concentration of alkaline activator can result in efflorescence, brittleness, higher porosity, and a reduction of overall mechanical properties and durability. This phenomenon can be traced to premature coagulation due to potentially faster dissolution of precursors in the mixture [109].

2.2.4. Mechanical properties of AAMs The mechanical properties of AAMs are mostly related to the activator content, curing regime, mixture's particle size distribution, and the chemical composition of the precursor(s). Since glass, as a precursor, has been reported to have a lower reactivity, the size of glass particles can be seen to have a definitive relationship with strength development. As a result, studies incorporating coarser glass particles (as in [113], [114]) experience higher overall mechanical properties reduction compared to those that used glass in finer particle sizes [21]. In micro-sized form, glass can enhance mechanical

properties by acting as a filler and reducing air-void pores, and if used in smaller particles, it can cooperate in hydration and geo-polymerization [47], [115].

2.2.5. Shrinkage of AAMs Shrinkage of portland cement concrete or AAMs is one of the major causes of cracking that allows transportation of moisture and deleterious ions into concrete structures. Shrinkage is generally categorized into drying shrinkage, plastic shrinkage, autogenous shrinkage, and carbonation shrinkage. Compared to conventional concrete, AAMs generally are known to have about 2-3 times higher drying shrinkage under ambient curing conditions [116]. Recent studies have shown that the use of high calcium precursors tend to result in a higher rate of drying and autogenous shrinkage [117]. This, however, is directly related to the rate of reaction, internal relative humidity, and surface tension of the pore solution. In that respect, internal curing, reduced Ca/Si ratio, as well as using shrinkage reducing agents are advised to reduce shrinkage [118]. Such methods, however, have been shown to not only reduce the strength gain, but also adversely affect setting time and modulus of elasticity [119], [120]. Yet, the influences of the type and content of the activators used have been reported to be more pronounced [121] with the higher content of activator generally resulting in higher overall autogenous shrinkage due to higher intensity of hydration. This phenomenon is associated with the increased consumption of moisture of the micropores and available content of silica that results in volume change [121].

2.2.6. Cracking potential of AAMs Although the bind-ability of AAMs is somewhat similar to portland cement concrete, due to the brittle nature of the produced paste, their tendency to crack is relatively higher. It is commonly known that the use of fibers [122], proper curing [123]–[126] and admixtures [120] can significantly reduce the brittleness of AAMs. Yet, the effect of glass powder on cracking potential of AAMs has not been investigated. Cracking of AAMs' samples can come from restrained drying shrinkage.

Shrinkage is a result of negative pressure build-up on capillary network. The high porosity of AAMs can lead to an increased evaporation rate of moisture, which in turn increases shrinkage, and thus cracking especially if the sample is restrained [127]. The cracking potential of AAMs depends on polymerization rate and the ambient condition that affects the drying shrinkage.

3. MIXTURE AND MATERIALS

The experimental program of this study is discussed in this section, which includes fresh, mechanical properties and cracking potentials of both normal and AAM mortars produced with glass powder.

3.1. Materials

3.1.1. Cement In this research study, Type I/II OPC with a density of 3.15 g/cm³ has

been used. Information on the physico-chemical properties of the OPC is provided by the supplier in Table 6.

Table 6. Physico-chemical properties of portland cement used in this study.

Physico-chemical properties of CEM I/II	
SiO ₂ (%)	20.8
Al ₂ O ₃ (%)	5.2
Fe ₂ O ₃ (%)	3.8
CaO (%)	64.3
MgO (%)	1.2
SO ₃ (%)	2.0
Na ₂ O (%)	0.1
K ₂ O (%)	0.4
LOI (%)	1.3
Specific surface area (cm ² /g)	3310
Density (g/cm ³)	3.15

3.1.2. Aggregate In this study, a local natural siliceous river with a specific gravity of 2.6 conforming to ASTM C33 [128] has been used. The sand in the mixes was added in saturated surface dry state to ensure that the test results were not affected through the absorption of moisture from the sands. Figure 1. shows the result of sieve analysis conducted based on ASTM C136 [1], and Table 7 presents the physical properties of the aggregates used in this study.

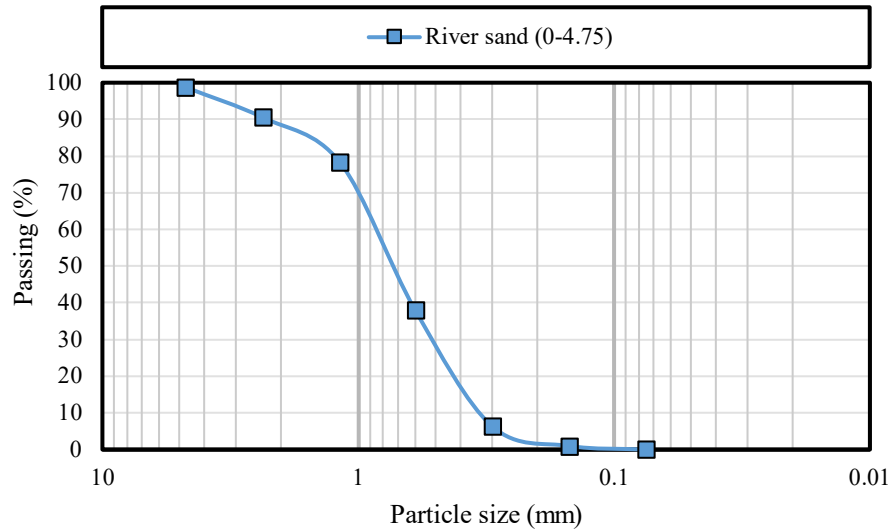


Figure 1. Sieve analysis of aggregates conducted based on ASTM C 136 [1].

Table 7. Physical properties of aggregates used in this study, based on ASTM C128.

Information	River sand
Bulk specific gravity	2.61
Apparent specific gravity	2.75
Water absorption (%)	1.93

3.1.3. Coal fly ash and GGBFS Coal fly ash (class F) used in this study was supplied from Boral resources originated from W.A Parish Plant Thompsons plant in Texas. GGBFS was supplied from Sky Cement Inc. located in Houston, Texas. Table 8 provides further details on the physico-chemical properties of coal fly ash used in this study.

Table 8. Physico-chemical properties of the coal fly ash and GGBFS used in this study.

Information	Fly ash (class F)	Blast furnace Slag (GGBFS)
SiO ₂ (%)	59.1	34.2
Al ₂ O ₃ (%)	20.7	13.6
Fe ₂ O ₃ (%)	5.6	0.7
CaO (%)	7.2	41.4
Na ₂ O (%)	1.3	-
K ₂ O (%)	1.2	-
SO ₃ (%)	0.8	-
MgO (%)	-	6.2
LOI (%)	-	-
Specific gravity	2.3	2.9
Moisture content (%)	0.09	-

3.1.4. Glass powder The glass powder used in this study was an ultra-fine-sized material a specific gravity of 2.6 and was supplied from Vitro-minerals – Tennessee, with a commercial name of VCAS™ 200. Table 9 provides information on the physico-chemical properties of the used glass powder provided by the supplier.

Table 9. Physico-chemical properties of glass powder

Physical properties		Chemical composition	
Specific gravity	2.6	SiO ₂ (%)	55-65
Bulk density	40-45	Al ₂ O ₃ (%)	10-15
Passing No. 325 Mesh, %	>99	Fe ₂ O ₃ (%)	<1
Median particle size d50, μm	6	CaO (%)	18-25
Pozzolanic strength index (10% portland cement replacement), % control	122	MgO (%)	2-5
Brightness %	87-90	Na ₂ O (%)	<4
Melting point, °C	1200	K ₂ O (%)	<0.2
Hardness	5.5	TiO ₂ (%)	<1

3.1.5. Superplasticizer In this study, to increase the flowability of the mixes, a polycarboxylic ether-based superplasticizer with a commercial name of Viscocrete 2100 was added to the mixes at a dosage of 1 vol% of the binder content for all the mixes.

3.1.6. Activator In this study, Reagent grade sodium silicate and sodium hydroxide supplied from Reagent Inc. and Duda Energy, have, respectively been used. The molarity of sodium hydroxide has been chosen as ten based on authors' experience in developing AAMs [17], [20], [24].

3.2. Mixture proportions

A total of four mixes, two geopolymer and two portland cement mortar, have been produced using coal fly ash (class F) and glass powder. In that respect, in each geopolymer mix, 50% glass powder or fly ash and 50% GGBFS has been used. In turn, in each Portland cement mortar, 25% coal fly ash or glass powder was used by mass volume, respectively. Table 10 provides further information on the mixture proportions whereby the mixes are labelled as follows letters GE, PC, FA and GP refer to geopolymer, portland cement, fly ash and glass powder, respectively. The number followed by each letter refers to the vol% of each material used in each mixture. For instance, PCFA25GP0 refers to a mixture, produced with portland cement that replaced by 25% fly ash and 0% glass powder. The reason for this proportioning is to see the pronounced effect of materials while not significantly affect the whole hydration process. In other words, the two mentioned content of 25 and 50% inclusion of glass powder in portland cement mortar and geopolymer mixes, respectively, is to evaluate a more realistic use of glass powder in the two binding systems.

Table 10. Mixture proportions.

Mixture name	L:B	SS/S H	SS (Kg/ m ³)	SH (Kg/ m ³)	M	OPC (Kg/ m ³)	FA (Kg/ m ³)	GGB FS (Kg/ m ³)	GP (Kg/ m ³)	RS (Kg/ m ³)	W (Kg/ m ³)	SP (Kg/ m ³)
PCFA25 GP0	0.4	–	–	–	–	448	116	–	–	1425	224	5.6
PCFA0G P25	0.4	–	–	–	–	448	–	–	109	1425	224	5.6
GEFA50 GP0	0.8	1	212	212	10	–	265	307	–	1402	–	–
GEFA0 GP50	0.8	1	212	212	10	–	–	307	258	1402	–	–

With L:B: liquid to binder ratio, SS: sodium silicate, SH: sodium hydroxide, OPC: ordinary portland cement, RS: river sand, GP: glass powder, W: water, SP: superplasticizer

3.3. Specimen preparation and test methods

In this study, the flowability, slump and flow table tests were conducted in accordance to ASTM C143 and ASTM C230, respectively. In addition, compressive, splitting tensile and elastic modulus tests were conducted according to ASTM C109, ASTM C496, ASTM C469, on $50 \times 50 \times 50$ mm cubes and 100×200 mm cylinders. To evaluate the shrinkage tendency of mixes, drying, autogenous and restrained shrinkage tests have been used. For the restrained shrinkage test, a customized ring, based on Ref. [129], has been produced by using a full bridge Wheatstone strain gauges to record the circumferential strain values of the steel ring. In all mixes and tests, ambient temperature curing of $23 \pm 2^\circ\text{C}$ with a relative humidity of $50 \pm 5\%$ has been adopted.

Table 11. Experiments conducted in this research along with other details.

Experiment	Standard	Specimen size (mm)	Time
Sieve analysis	ASTM C136 [1]	–	–
Slump test	ASTM C143 [130]	–	–
Flow table	ASTM C230 [131]	–	–
Fresh density and air content	ASTM C138 [132]	–	–
Compressive strength	ASTM C109 [133]	50 × 50 × 50	7, 14, 28, 56
Splitting tensile strength	ASTM C496 [134]	76 × 152	28
Elastic modulus	ASTM C469 [135]	76 × 152	28
Abrasion resistance	ASTM C944 [136]	100 × 200	28
Electrical resistivity	ASTM C1876 [137]	100 × 200	28
Water absorption and apparent porosity	ASTM C20 [138]	50 × 50 × 50	28
Drying shrinkage	ASTM C157 [139]	76 × 76 × 280	3, 7, 14, 28, 56
Autogenous shrinkage	ASTM C157 [139]	76 × 76 × 280	3, 7, 14, 28, 56
Restrained shrinkage	ASTM C1581 [140]	–	–

3.3.1. Fresh property tests To ensure consistency, the mixtures were tested using a mini slump, flow table, air content and fresh density fixtures. Each test has been conducted two times to ensure the values are correctly documented. Such tests were conducted to provide details on workability to avoid potential issues in the hardening stage.

3.3.1.1. Slump test The slump test is a basic consistency of fresh concrete (or mortar) test conducted on fresh mixture. Slump is most commonly performed to check the workability of the freshly mixed concrete to show how easy the mixture flows. This standard test is specified by ASTM C143 for normal concrete and ASTM WK63516 for mortar and paste [130]. In this research, since mortar samples were used, mini slump test was conducted whereby the drop in mixtures' height were measured.

3.3.1.2. Flow table test The flow table test can potentially determine the consistency and flowability of cement mortar, which is listed in the ASTM C1437 [130]. Using this test, the dimensions of the flowed concrete mortar, as well as any indication of segregation, is determined. The flow table has an approximately 254 mm (10 in) sized diameter with a cast bronze flow mold 70/102 mm top/bottom diameter.

3.3.1.3. Air content and fresh density Air content and fresh density of mixtures conducted based on ASTM C138 [132]. The air content was measured with a pressure meter as described in ASTM C138. The fresh density was tested with a fixture having a volume of 0.250 ft³ which is equal to 0.00707 m³.

3.3.2. Hardened properties tests Hardened concrete requires to have adequate strength and stiffness to withstand service loads. Several common tests for hardened properties were conducted in this study for which at least 3 specimens were produced and tested. The results are outlined in the below subsections.

3.3.2.1. Compressive strength test The compressive strength test is the most common mechanical property test to characterize concrete's ability to sustain compressive loadings. The standard test is specified by ASTM C109 whereby the samples are subjected to compressive loads until they break apart. In this study, 50 × 50 × 50 mm cube samples were tested under an applied loading rate of 0.25 ± 0.05 MPa/s (35 ± 7 psi/s) after 3, 7, 14, 28, 56 days of curing.

3.3.2.2. Splitting tensile strength The splitting tensile test was conducted using cylinder samples conforming to ASTM C496 at the ages of 3, 7, 14, 28, 56 days. The cylinders had a dimension of 75 × 150 mm (3 × 6 in.). During the test, the applied

load ranged from 0.7 to 1.4 MPa/min and two plywood strips with a thickness of 3 mm were used.

3.3.2.3. Elastic modulus Elastic modulus (also modulus of elasticity) is a measure of a material's ability to resist deformation under stress. The standard test method was based on ASTM C469, whereby cylinder-shaped specimens with a dimension of 75 × 150 mm (3×6 in.) and their respective displacement were recorded by linear variable differential transformer (LVDT). The loading rate was at a constant level within the range 250 ± 50 kPa/s [35 ± 7 psi/s]. After 3, 7, 14, 28, 56 days, the elastic modulus of samples cured under ambient temperature were tested and documented.

3.3.3. Abrasion test Abrasion resistance is one of the major properties of concrete members especially those that are exposed to friction forces such as skidding, rubbing and sliding [141]. According to Ref. [142], several ASTM abrasion procedures are developed to assess the abrasion resistance of hardened concrete. ASTM C418, ASTM C779, ASTM C944 and ASTM C1138 are among the most commonly used procedures to evaluate the abrasion properties of concrete, which simulate traffic effects through sandblasting, revolving disk machine, rotating cutter, and abrasive action of water-borne particles, respectively.

The abrasion test that was conducted in this research was based on ASTM C944 [136] that used a rotating cutter drill press. This test method evaluated the relative wear resistance of mortar utilized in quality control of highway and bridge pavement concrete subjected to traffic by documenting the weight loss of specimen on a 2-minute time

interval. The purpose of this test was to further assess the feasibility of using mortar samples containing glass powder in surface layers such as pavement surface courses.

3.3.4. Water absorption and apparent porosity To evaluate the water absorption and apparent porosity of the mixes a total of 36 cubic samples have been made. The specimens were tested in three different curing conditions of ambient temperature (23°C with RH 50%), oven curing (at 110°C with RH 50%) and moist curing (23°C with RH 100%) tested according to ASTM C20 [138] for water absorption and apparent porosity. In this test, initially mortar cubes are produced and demolded after 24 hours of initial curing. After 28 days of curing, specimens are dried in 110C for about 24 hours and weighted as dry weight (D). Followed by this, specimens are put in water to boil for 2 hours and then kept in room temperature while still being immersed in water to cool down. Before weighing the saturated specimen, they should be kept in water for a minimum of 12 hours. The value recorded should be considered as suspended weight (S). After weighing the samples, they should be cleaned lightly by a cloth to remove all the drops of water from the surface and weighed as saturated weight (W). After this, the specimens' apparent porosity and water absorption can be calculated as in Eq. 2 and Eq.3, respectively, as the following:

$$P (\%) = [(W-D)/V] \times 100 \quad (\text{Eq. 2})$$

$$A (\%) = [(W-D)/D] \times 100 \quad (\text{Eq. 3})$$

3.3.5. Drying shrinkage Drying shrinkage is one of the most commonly observed shrinkage types for AAMs. The drying shrinkage test was performed based on ASTM C596 using $25 \times 25 \times 285$ mm prism specimens. In this test, after pouring the molds with mortar, the specimens were allowed to cure for a period of 24 hours while their surface was sealed by a plastic cover and wet burlap at the room temperature. After that, the specimens were removed from the mold and were placed in a standard dry condition ($23^{\circ}\text{C} \pm 2^{\circ}\text{C}$ with RH of 50%) using an environmental chamber. The length change and mass loss of specimens were recorded after 3, 7, 14, 21, 28, 56 days of curing.

3.3.6. Autogenous shrinkage To measure autogenous shrinkage of AAMs specimens, $25 \times 25 \times 285$ mm prism specimens were used. After 24 hours, specimens were demolded and then immediately sealed with four layers of adhesive back aluminum foils. This could avoid moisture exchange with the surrounding environment. The specimens were then put in the environmental chamber with a constant temperature of $23^{\circ}\text{C} \pm 2^{\circ}\text{C}$ and a RH of 50%. The length and mass changes of specimens were then recorded after 3, 7, 14, 21, 28, 56 days.

3.3.7. Restrained shrinkage Since free shrinkage only provides insight into the extent of length change in an unrestrained condition, it does not provide a direct measure of the cracking potential of the material under restrained conditions. In other words, the cracking style, duration and their propagation can provide further information on the potential failure style of concrete structures produced with such materials.

It is commonly established that the failure can be based on brittle failure, elasto-plastic fracture or plastic collapse [143]. As reported by Ref. [144], avoiding a single plastic failure can enhance structural safety and allow more time for failure detection. Nonetheless, although there are other methods of evaluating such properties, crack propagation and their respective size can provide information on the mentioned as well. In this regard, this study directly measured the cracking potential of the studied materials based on a restrained shrinkage test. The restrained shrinkage test, with a modified geometry from ASTM C1581, used two rings with an approximated diameter of 95 and 150 mm (3.75 and 6 in.), respectively; one ring is made of a steel tube (the inner ring) and the other (outer ring) is made of plastic mold. The reason for this modification is due to significantly reducing the cracking time as noted in Ref. [144]. Notably, other studies such as Refs. [145], [146] also proposed their own versions of modified ASTM C1581 restrained shrinkage to reduce the cracking time. In this research, the fresh mortar was cast into the space between the two ring molds. After sealing the top of the rings and allowing them to be initially cured for 24 hours, the outer ring mold was removed. This exposed the outer most section of the mortar to the surrounding environment, inducing drying shrinkage. During the test, the top and the bottom of the ring were sealed to ensure that no drying takes place from those two sides. As the mortar dries, it induces internal stress which is due to the resistance of the steel ring. To record this process, four strain gauges were attached to the inner radial surface of the steel to record the circumferential strain. Based on the strain history, a sudden drop in strain indicated that the mortar ring cracked. As

shown in Ref. [144], the modified ring geometry is effective in significantly reducing the cracking time of mortar compared to other ring tests. The strain gauges used in this test were 6.2-mm, 350-Ohm strain gages patterned in full Wheatstone bridge with two Poisson gages and two linear gages [129], [147]. The D4 data acquisition unit was supplied from Micro-measurement Inc. and recorded the strain in 2-minute intervals. Figure 2 (a) presents the orientation of strain gauges used in this study. Figure 2 (b) shows the cast ring with its surface covered with aluminum foil to avoid moisture loss at initial 24 hours of casting. Further, as can be seen in Figure 2 (c), the outer cover is removed and the rings are placed in an environmental chamber. To avoid the effect of air flow within the chamber, a storage container was used to cover the rings.

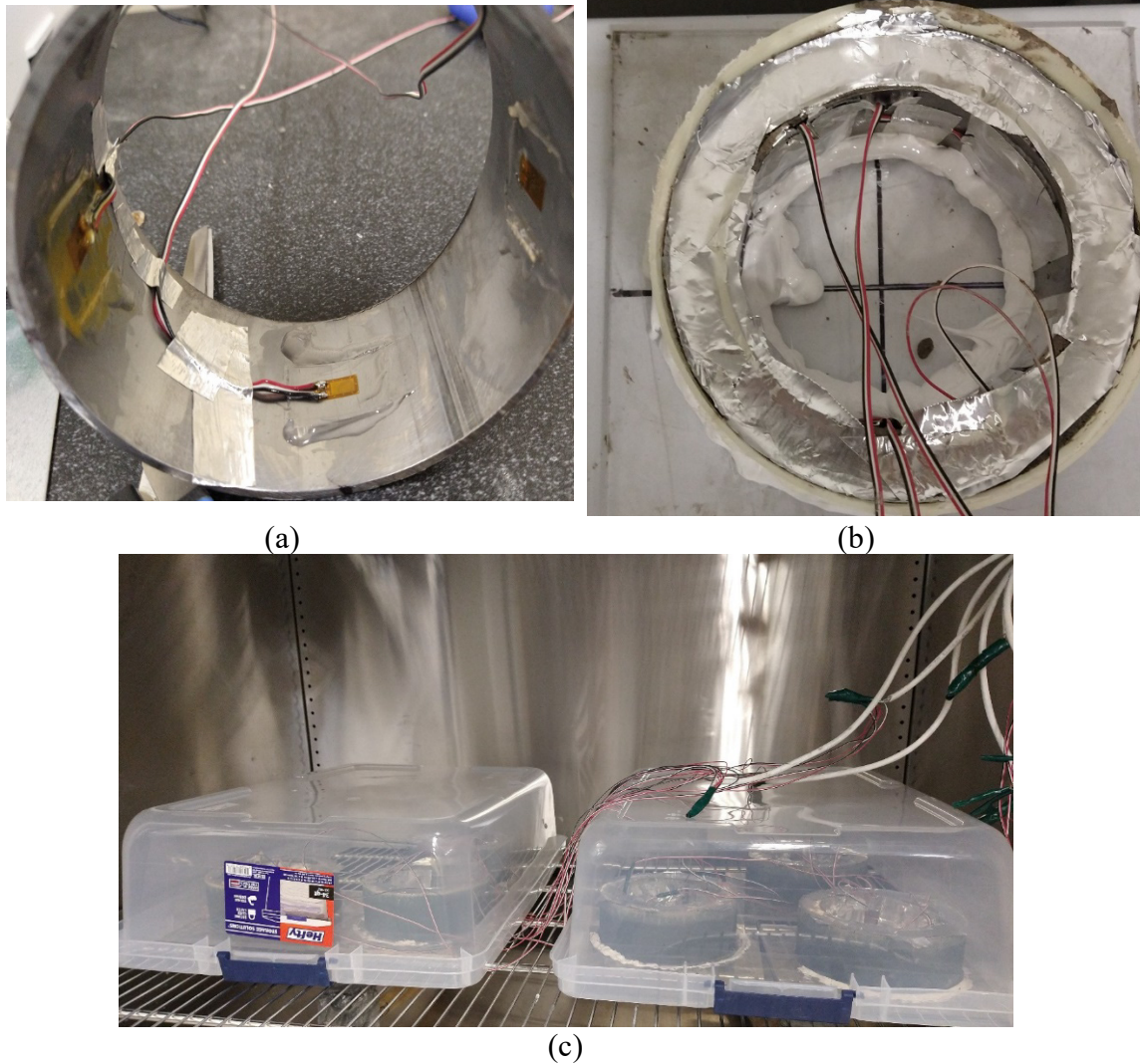


Figure 2. the test set up of restrained shrinkage fixtures showing: (a) orientation of strain gauges, (b) covering the surface of hardened concrete to avoid moisture evaporation, (c) use of storage cover on rings to avoid air flow effect on recording.

3.3.8. Electrical resistivity In this study, electrical resistivity of concretes after 28 days of curing has been evaluated based on ASTM C1202 [148]. In this method, a specific fixture was used to test 150×300 mm samples' resistivity based on electrical current that is applied to the moist concrete samples.

3.3.9. Surface morphology In this study, to evaluate the surface properties of the produced specimens Hirox Digital Microscope has been used. This microscope has the capability of taking up to 2500X magnification at a high resolution of 10560×6600 with processing algorithms for anti-halation, contrast, edge, and hue/chroma correction. As for the specimen, it was cut about 2 inches from the top of a 76×152 mm cylinder with a smooth surface.

4. TEST RESULTS AND DISCUSSION

The experimental program conducted in this study included a series of physico-mechanical and cracking potential tests. The following sections further elaborate on each property as tested.

4.1. Flowability

Figure 3 presents the result of mini-slump and flow table tests conducted on various mixes. From this figure, the highest and lowest values of flow table are for PCFA0GP25 and GEFA0GP50. In that respect, portland cement mortar mixes are found to have a relatively higher flowability values which can be due to the inclusion of 1 vol% superplasticizer. In terms of materials, however, it is notable that the inclusion of glass powder has slightly increased the flowability of portland cement mortar mixes. Previous studies, such as Refs. [149]–[151] have noted that due to impermeability and smooth (glassy) surface of glass particles, it can increase the flowability of mixes. As reported by Ref. [152], the inclusion of glass powder can reduce the initial and final setting time of mixes but it also increases the flowability of materials.

Yet, the effect of glass powder on geopolymer mixes is found to be opposite and has lowered both mini-slump and flow table values. According to Ref. [152] the better performance of glass powder in normal portland cement mortar is due to the high adsorption of superplasticizer on glass particles that has substantially increased the initial flowability values. Ref. [152] associated this to the electrostatic attraction of positive and negative charges of Ca^{2+} and Si-O^- , respectively. On average, however, mixes with glass powder are found to have 3% lower flowability values which can be due to its high angularity, compared to coal fly ash particles. Further from Figure 3, the mini slump

values also show a similar trend, compared to flow table that the inclusion of glass powder has reduced the geopolymer mixes while it has increased the flowability of portland cement mixes. In this regard, the highest and lowest mini slump values is 142 mm for PCFA0GP25 and 134 mm for GEFA0GP50, respectively. Nonetheless, it should be noted that the difference between values is not statistically significant, thus, essentially all mixes had a rather similar level of consistency.

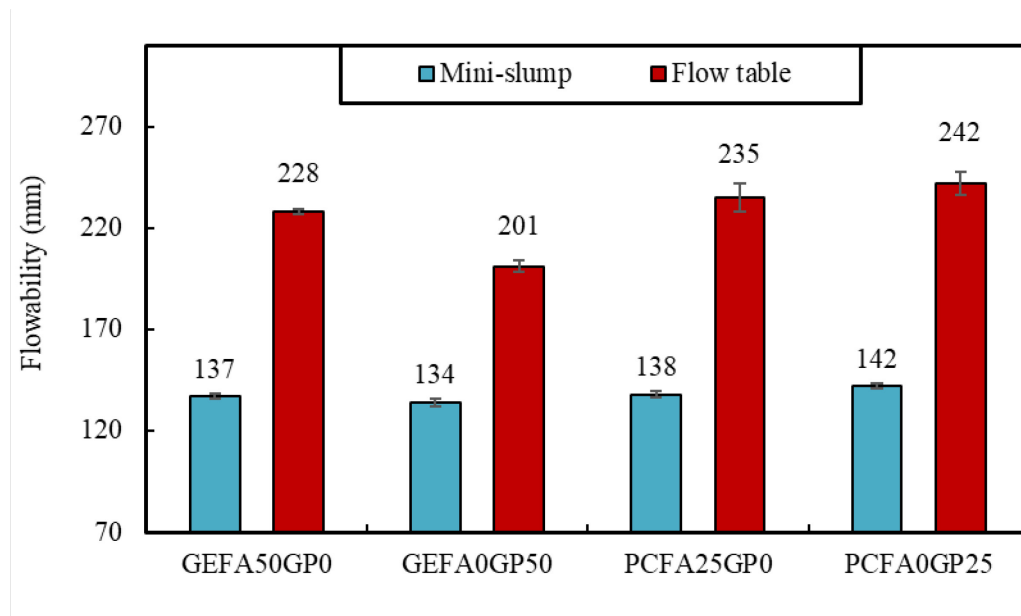


Figure 3. Flowability of mixes.

4.2. Air content

Figure 4 presents the result of air content for all mixes. The highest and lowest air content values are 6.4% for GEFA0GP50 and 3.1% for PCFA25GP0, respectively. In addition, geopolymer mixes have a mean air content value of 6.3% while portland cement mortar mixes have a mean air content of 3.4%. This shows that geopolymer mixes have about 46% higher air content which can explain the generally perceived higher porosity of geopolymer mixes, as explained in Refs. [17], [24]. Furthermore, although the difference between the values is not statistically significant, mixes containing glass

powder have about a mean air content value of 8% higher than those containing fly ash (class F). This can be due to lower particle flowability of mixes containing glass powder due to its angular shape, compared to coal fly ash [21].

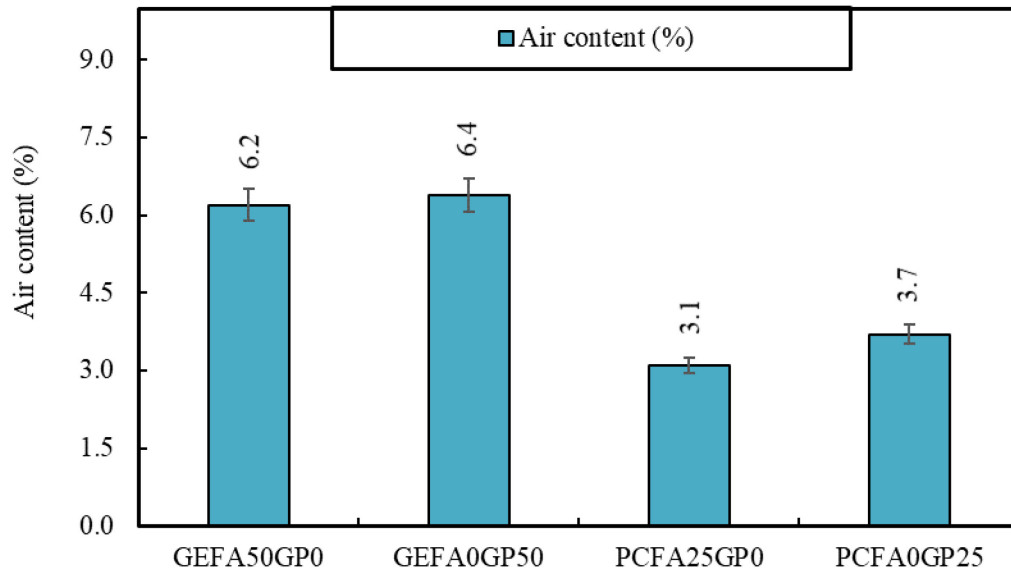


Figure 4. Air content of mixes.

4.3. Fresh and hardened density

The result of fresh and hardened densities (28 days) of mixes is presented in Figure 5. Based on this figure, the fresh density values of geopolymer mixes are found to be relatively lower than those of portland cement mortars. In that respect, the mean value of the fresh density of geopolymer and portland cement mortars are found to be 2133 kg/m³ and 2278 kg/m³, respectively. The higher fresh density values of portland cement mixes can be due to lower air content, as discussed in the section 4.2. A similar trend can be seen for hardened density. Although the mixes containing glass powder developed a relatively lower fresh density values, their hardened density is found to be higher than the

mixes produced with fly ash. This can be due to potentially enhanced reactivity of mixes containing glass powder that makes the microstructure denser.

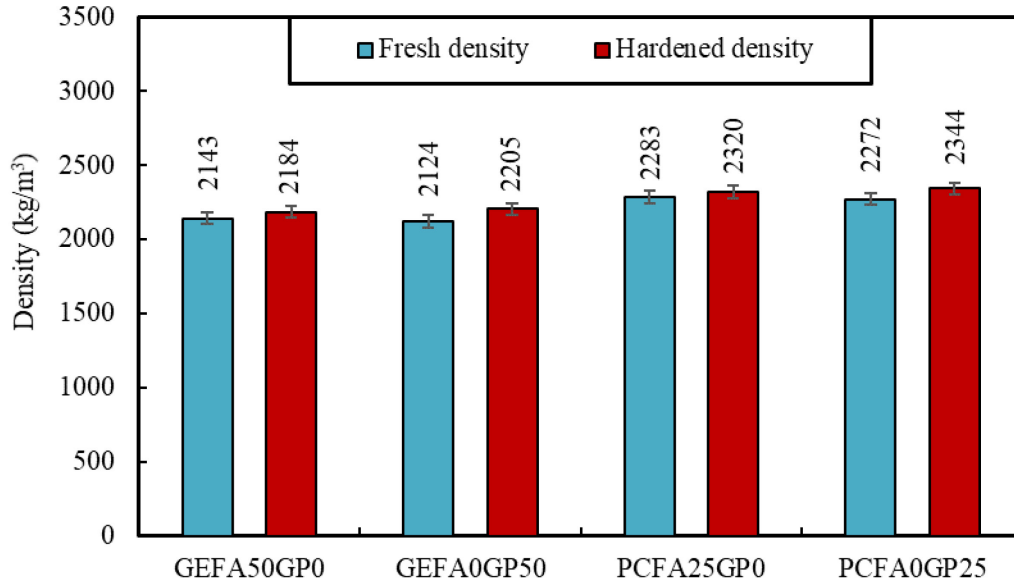


Figure 5. Fresh and hardened density of mixes.

4.4. Compressive strength

Figure 6 provides the result of compressive strength conducted on the specimens after 3, 7, 14, 28 and 56 days of curing. Based on this figure, in general, geopolymer samples outperformed those of portland cement mortars in both control and glass powder containing mixes. In addition, the range of compressive strength values is found to be from 13.7 MPa for PCFA25GP0, after three days of curing, to 56.2 MPa for GEFA50GP0, after 56 days of curing. Based on this figure, the geopolymer mixes containing glass powder had a relatively lower strength values potentially due to lowered reactivity rates of glass powder when used at higher quantities. As reported by Refs. [47], [57], this can be due to the effect of higher content of SCMs in hydration (in this case, geopolymerization) kinetics.

In portland cement mixes, however, glass powder is found to perform considerably better with an average compressive strength of 31 MPa versus 19.2 MPa achieved for mixes containing 25% coal fly ash which can be due to the ultra-fineness of fly ash particles increasing reactivity values. This difference in the performance in the two binding systems shows that the higher Al ratio of fly ash (class F) plays a key role in the enhanced geopolymerization. Similarly, in a research conducted by Ref. [115], it was reported that the inclusion of glass powder increases the Si/Al ratio which can significantly lower the initial strength gain of geopolymer mortars. Ref. [151], also noted similar results in portland cement mortar and associated the reactivity rate of glass powder to be significantly affected by the surface area and particle size of the glass powder.

In either binding system, however, the mean value of all mixes containing coal fly ash (3, 7, 14, 28 and 56 days) is found to be 33 MPa which translates into 14% decrease from 38 MPa mean value of mixes containing glass powder. The better performance of mixes containing glass powder in portland cement mortar can be due to the pozzolanic reactivity of glass particles.

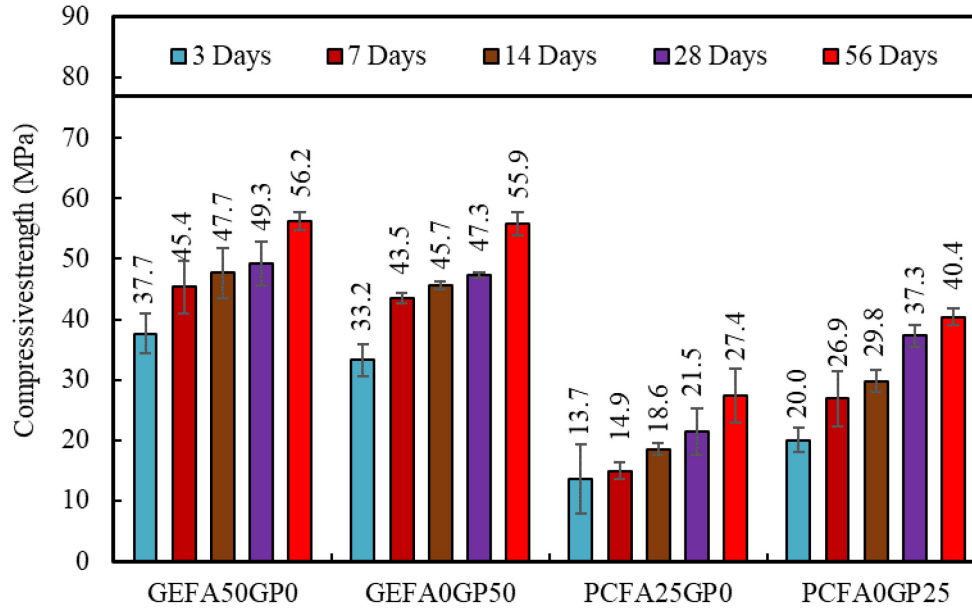


Figure 6. Compressive strength of mixes.

4.5. Splitting tensile strength

Figure 7 presents the splitting tensile strength values of various mixes tested up to 56 days of curing. According to this figure, it is evident that mixes containing glass powder have outperformed their companion mixes with fly ash in portland cement system. In this regard, the mean value of portland cement mortar mixes containing 0 and 25% glass powder is found to be 3.1 and 3.9 MPa, respectively. The better performance of glass powder containing mortars is similar to the results outlined in compressive strength. Unlike glass' effect on portland cement mortar, in geopolymer mixes, based on Figure 7, the inclusion of glass powder has lowered the strength values by about 15%. According to Ref. [153] this can be due to the increase in air-void content of mixes containing glass powder, which is aligned with the findings reported in section 4.2.

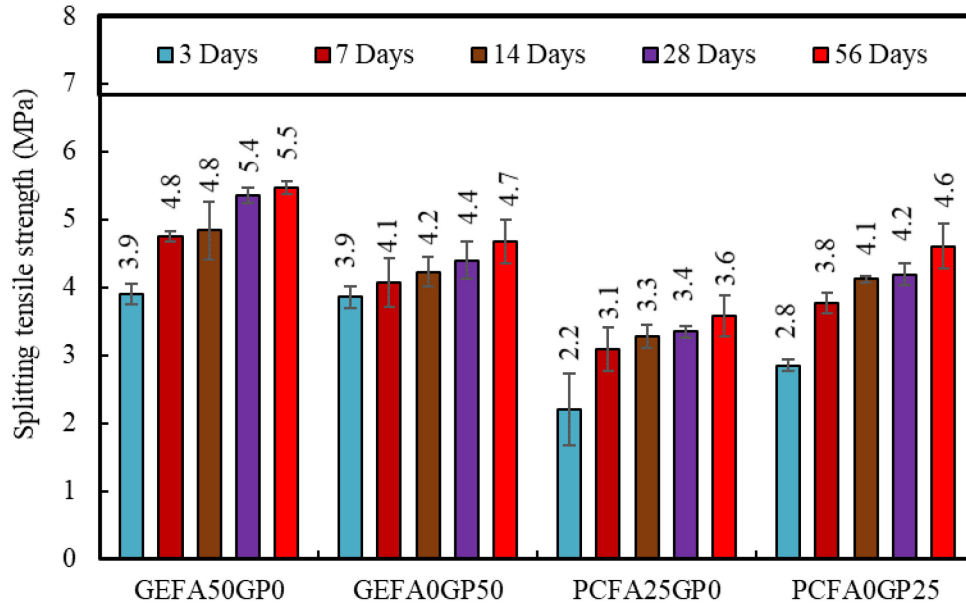
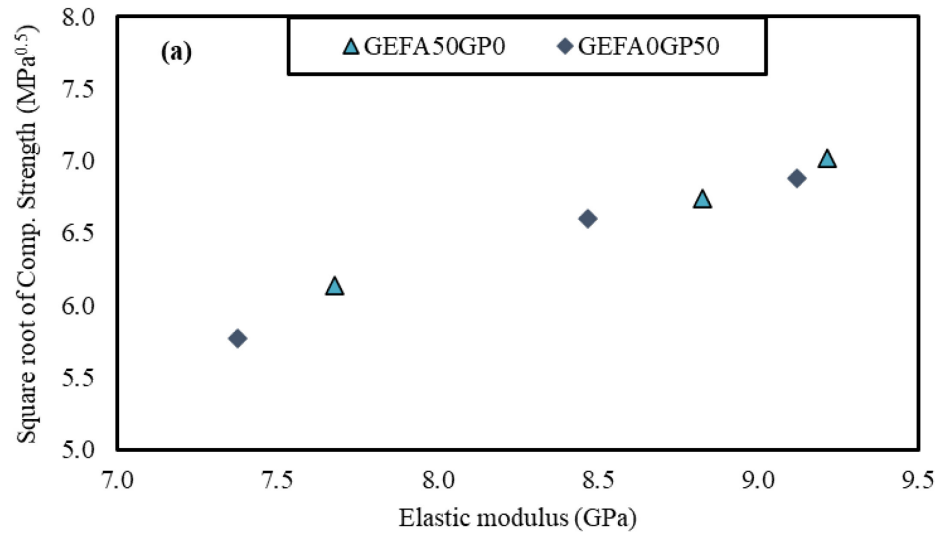
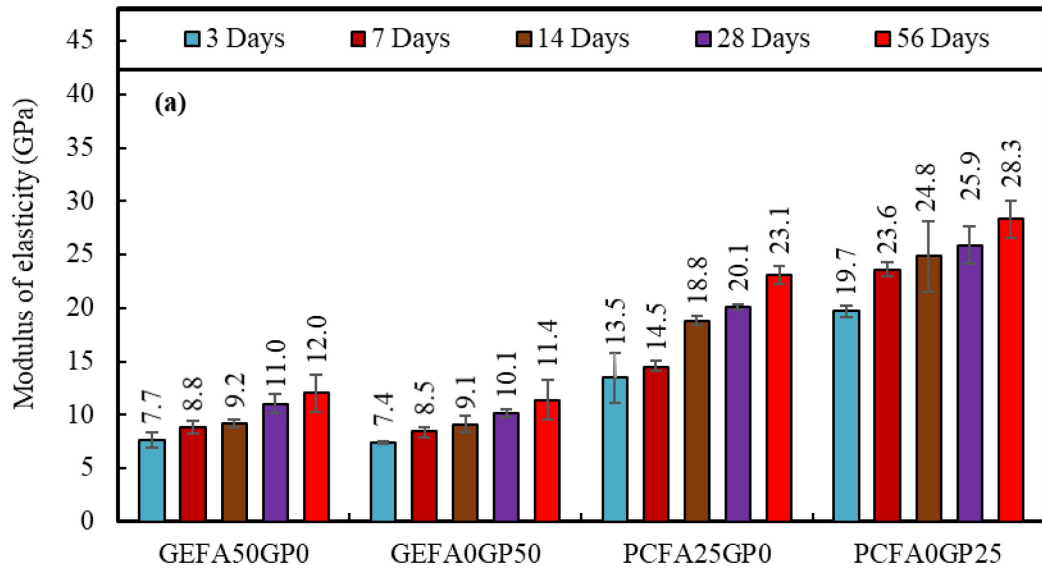


Figure 7. Splitting tensile strength of mixes.

4.6. Elastic modulus

The result of elastic modulus test conducted after 3, 7, 14, 28 and 56 days of curing is presented in Figure 8. Based on this figure, the elastic modulus ranged from 7.4 GPa for GEFA50GP0 to 28.3 GPa for PCFA0GP25. As can be seen in this figure, despite the higher compressive strength values of geopolymer mortar discussed in section 4.4, their elastic modulus values are significantly lower than portland cement mortars. The reason for this is discussed at length in Refs. [17], [24]. Further, mixes containing glass powder are found to have a lower modulus of elasticity values in geopolymer mortar. Yet, in portland cement mortar mixes, higher modulus is achieved. This can be rooted in the binding mechanism of AAMs and its higher porosity [150]. Figures 8 (b) and (c) present the comparative values of the square root of compressive strength versus elastic modulus. In both figures, as the square root strength increases, the elastic modulus values also increase.



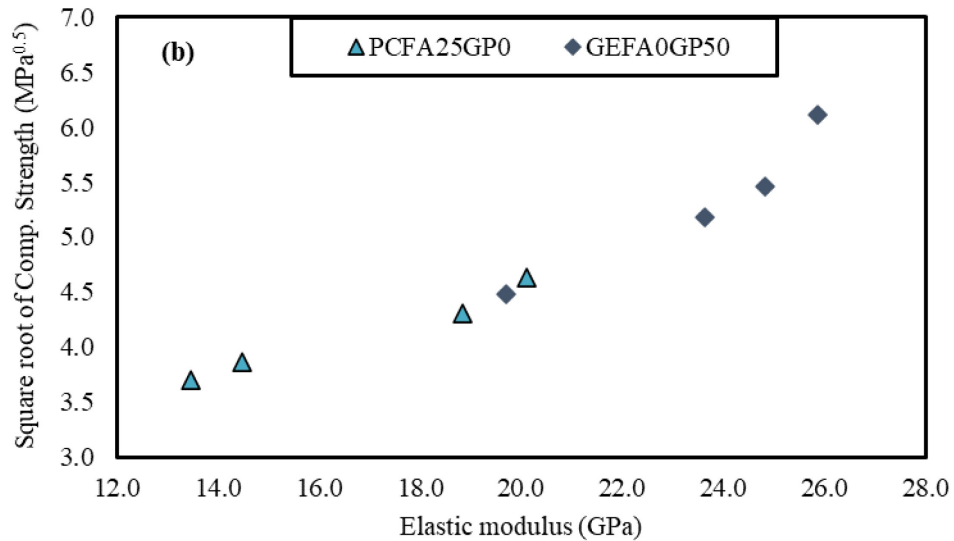


Figure 8. The result of (a) elastic modulus, (b) and (c) comp. strength to elastic modulus.

4.7. Abrasion resistance

Abrasion resistance presents the ability of a given material to withstand the deteriorating effects of friction. The result of 28 days mass loss of specimens is sketched in Figure 9. Based on this figure, in the geopolymer mixes, GEFA0GP50 is found to have the lowest mass loss which is 45% lower than its companion mix with 50% fly ash. This can be due to the high hardness of the used glass powder, as reported in Table 9. Similarly, in portland cement mortar specimens, mixes containing fly ash are found to experience about 9% higher mass loss. Based on the results, geopolymer mixes containing glass powder have outperformed all other mixes in abrasion resistance. Similar findings have been documented by Ref. [154] when glass powder is added to the mixes.

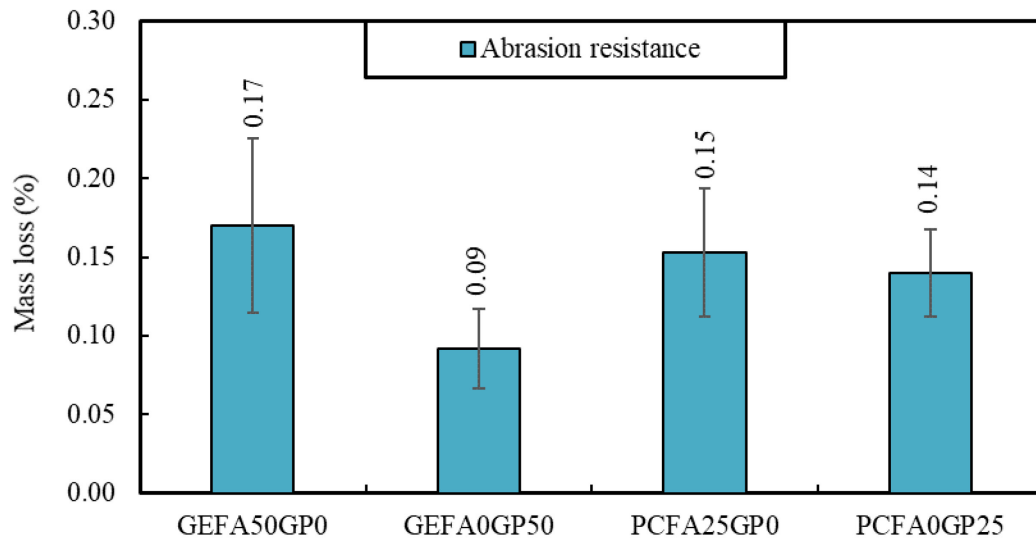


Figure 9. Abrasion resistance of mixes.

4.8. Water absorption and apparent porosity

Figure 10 presents the result of water absorption and apparent porosity of mixes cured in three different curing regimes and tested after 28 days. As can be seen in Figure 10 (a), the highest and lowest water absorption is for GEFA0GP50 with 11.3% and PCFA0GP25 with 4.3%. Further, geopolymer samples containing glass powder are found to have a slightly higher value of water absorption (9.7%) compared to geopolymer samples made with 50% fly ash (with 9.6%). Unlike in geopolymer mixes, however, the mean water absorption value of portland cement mortars is found to be considerably lower, in any of curing regimes. In that respect, mixes containing glass powder, are found to have developed lower overall water absorption with the mean value of 5.2% compared to 6.6%, respectively. The reason for this can be the effect of superplasticizer on portland cement mortar's rheology that can significantly increase its flowability but has no effect on its initial or final setting time [152]. Similar to water absorption results, the result of porosity values show mixes produced with geopolymer system have higher porosity

which is not only because of air-void pores but also gel pores and capillary pores [17], [24]. In either case, moist cured specimens have developed higher water absorption and porosity in geopolymer mortar mixes. The reason for this can be due to the effect of moisture on dilution of alkalinity, as reported in Ref. [17]. Nonetheless, moisture curing is found to perform considerably better in portland cement mortar mixes potentially due to enhanced hydration. Most notable of all, however, in either system, exposure of glass containing mixes to thermal curing has slightly performed better than those produced with fly ash. The reason for this can be the lower sensitivity of glass powder to thermal stress. Thermal stress, according to Ref. [17] can produce micro cracks that results in larger pores. The reason for better performance of glass powder can be its production process that it is exposed to very high temperatures (up to 1400°C). In addition, glass powder is considered to be a ceramic material and as discussed by Refs. [19], [21], ceramics generally have a very high thermal resistance. Nonetheless, it is worth noting that since the mentioned results are reported based on ASTM C20, basically the surface porosity plays a significant role in the reported values. Further studies in this area, possibly utilizing computerized tomography (CT scan) to evaluate the comparative thermal performance of the two materials can provide further details on pore formation and connectivity.

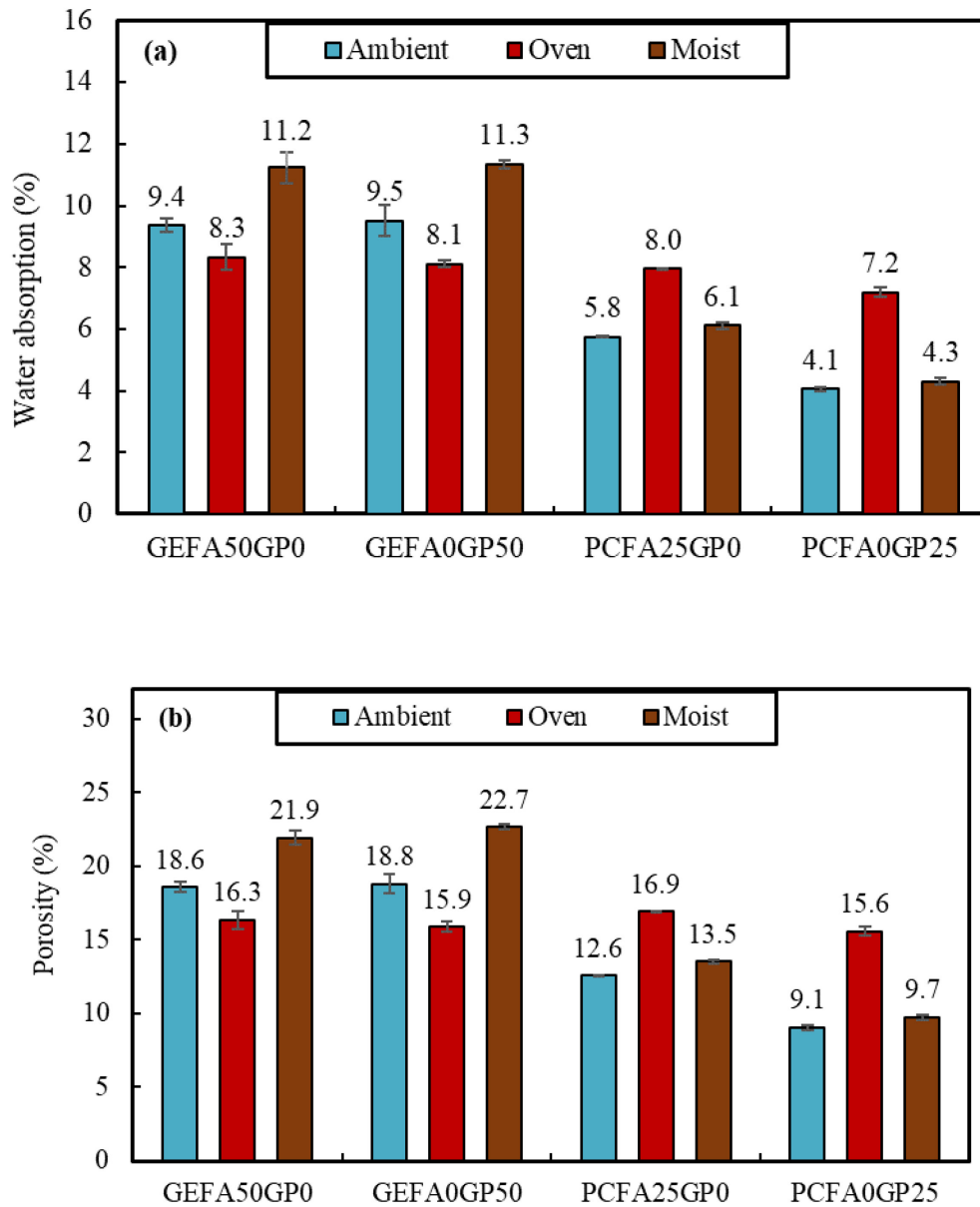


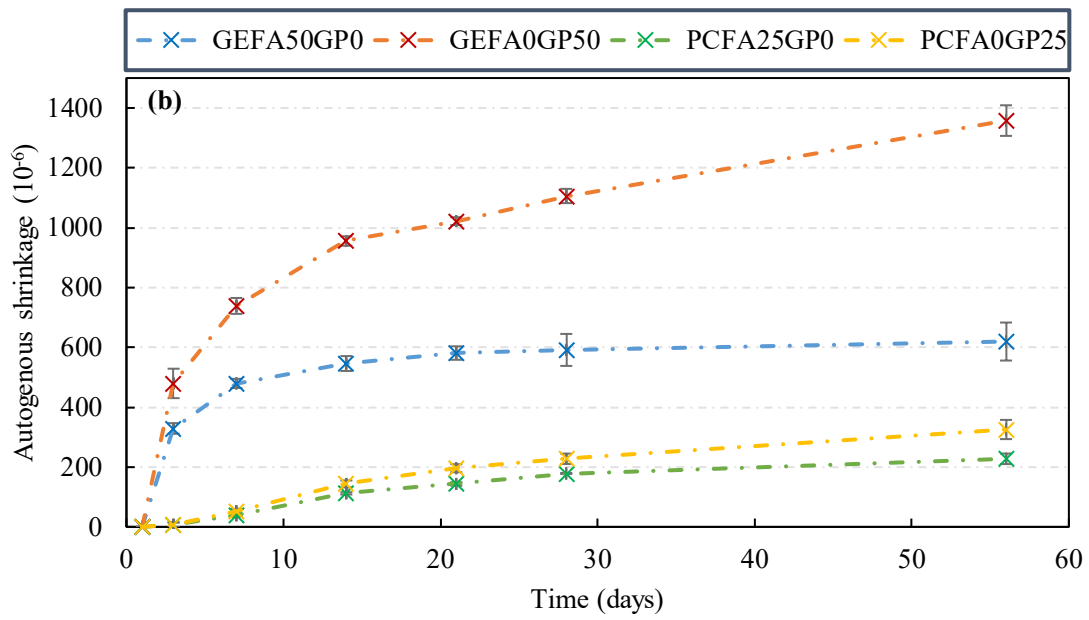
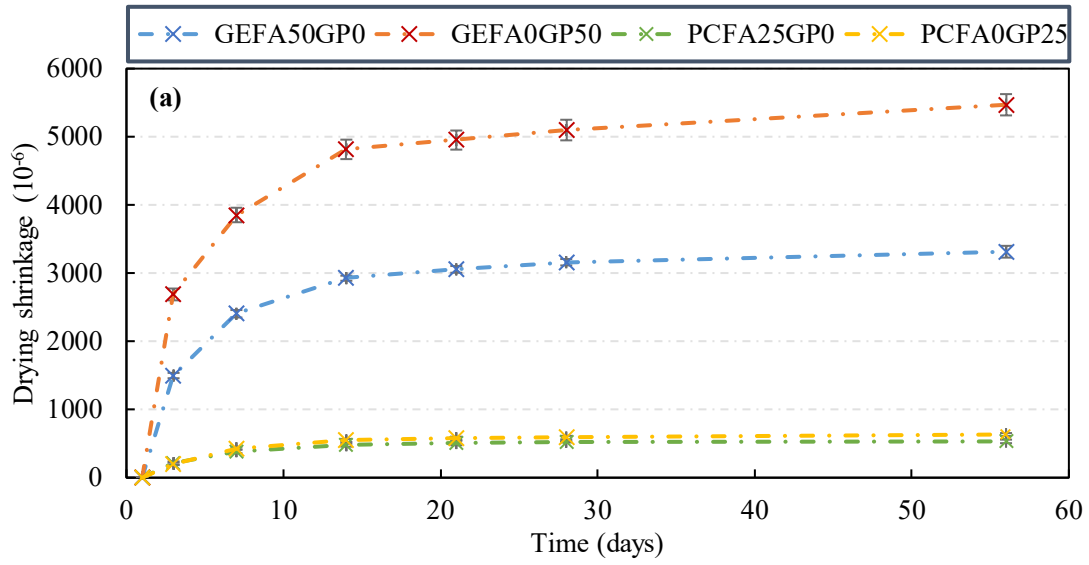
Figure 10. The result of (a) water absorption and (b) apparent porosity of mixes.

4.9. Drying and autogenous shrinkage

The result of drying and autogenous shrinkages until the 56th day of curing is presented in Figure 11 (a) and (b), respectively. Figure 11 (a) shows GEFA0GP50 has the highest (5384.6 $\mu\epsilon$ at the 56th day) and PCFA25GP0 has the lowest (193.35 $\mu\epsilon$ at the 3rd day) drying shrinkage strain values. In general, the mean drying shrinkage values of

mixes containing glass powder is 2444.5 $\mu\epsilon$ versus 1584.1 $\mu\epsilon$ for mixes containing fly ash, which means the inclusion of glass powder has caused a 54% increase in the micro strain values, irrespective of the binder type. The higher micro strain values of mixes produced with glass powder is due to higher surface area and reactivity that results in higher shrinkage. According to Ref. [34] this is due to the water absorption mechanism of glass powder that when it reacts results in higher self-desiccation.

Further from Figure 11, the geopolymer mortars appear to have a mean micro strain of 3551 $\mu\epsilon$ while portland cement specimens have a value of 477.6 $\mu\epsilon$. This shows a 640% increase in the micro strain values of geopolymer mixes which is exacerbated by about 38% by the inclusion of glass powder. This can be due to the lower modulus of elasticity of geopolymer samples, discussed in section 4.6, as well as higher air content of geopolymer mixes that results in lower content of solid content to withstand the contracting force of shrinkage [13]. This finding is also aligned with those of Ref. [155]. In general, however, it is believed that the higher shrinkage tendency of mixes containing glass powder is, in fact, resulted from autogenous shrinkage. Autogenous shrinkage is commonly resulted from the hydration process. Since no microstructural analysis is conducted in the presented research, the evaluation of the difference between the unhydrated versus hydrated products are not made. Thus, the shrinkage resulted from hydration is only evaluated in terms of length change which can take place due to a combination of types of shrinkage. Nonetheless, comparing the Figures 11 (a) and (b), the trend of all specimens is similar and point to the higher length change of mixes containing glass powder.



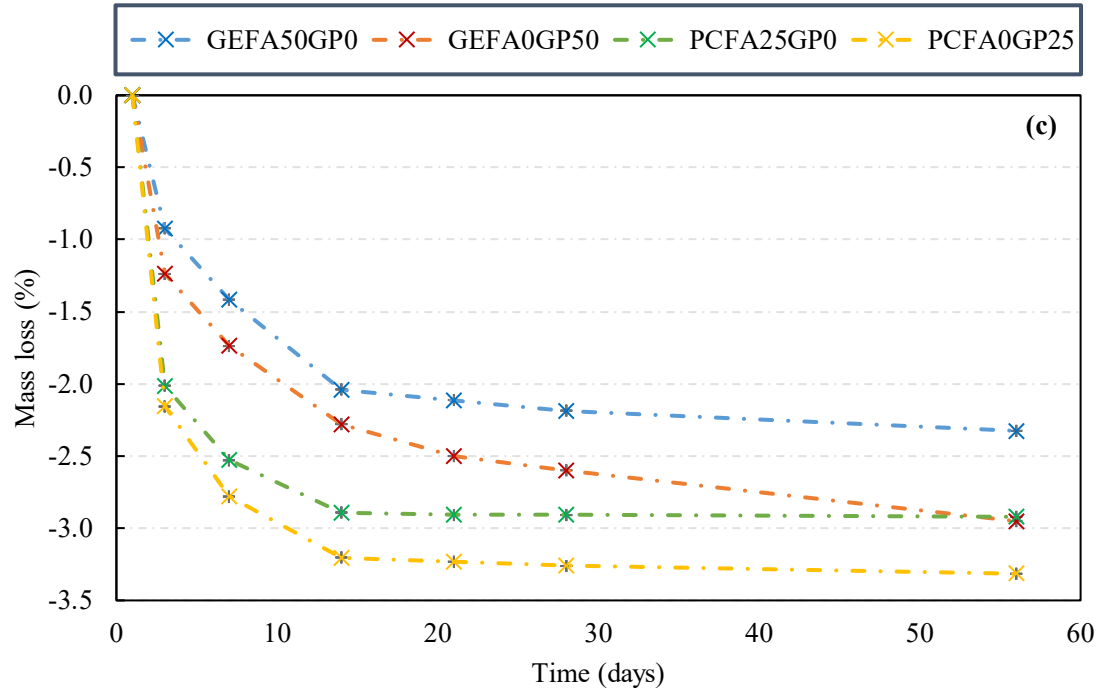


Figure 11. The result of (a) autogenous shrinkage, (b) drying shrinkage and (c) mass loss of mixes exposed to drying shrinkage condition.

4.10. Restrained shrinkage

The result of restrained shrinkage test is presented in Figure 12. The geopolymer samples developed considerably higher initial strain values that leads to rapid initial cracking, which was due to high autogenous and drying shrinkages. Further from Figure 12, the geopolymer mortar samples containing fly ash have continued at a rather similar strain rate while samples produced with glass powder have been increasing the strain values even after 11 days of curing. This can be due to the very high shrinkage of geopolymer mixes that led to multiple cracking with a relatively higher width to take place on the top surface of the geopolymer samples (see Figure 13 (GEFA50GP0 and GEFA0GP50)). Despite such high strain values, since the type of cracking is different due to lower modulus, the strain values are seen to continue to increase over time and not behave as portland cement mortar that suddenly drops.

Further from Figure 12, unlike in geopolymer samples, portland cement mortars produced with and without glass powder (PCFA0GP25 and PCFA25GP0) experienced a sudden drop in their strain values when cracked. This shows a totally different cracking behavior for samples made with geopolymer versus portland cement mortar, as well as those produced with and without glass powder. Table 12 summarizes the result of restrained shrinkage tests conducted using various mixes. Based on Table 12, the size of geopolymer samples ranged from 1 mm to 2 mm with the larger sizes for samples made with glass powder. As for normal portland cement mortar samples, relatively similar results have been achieved for specimens made with and without glass powder.

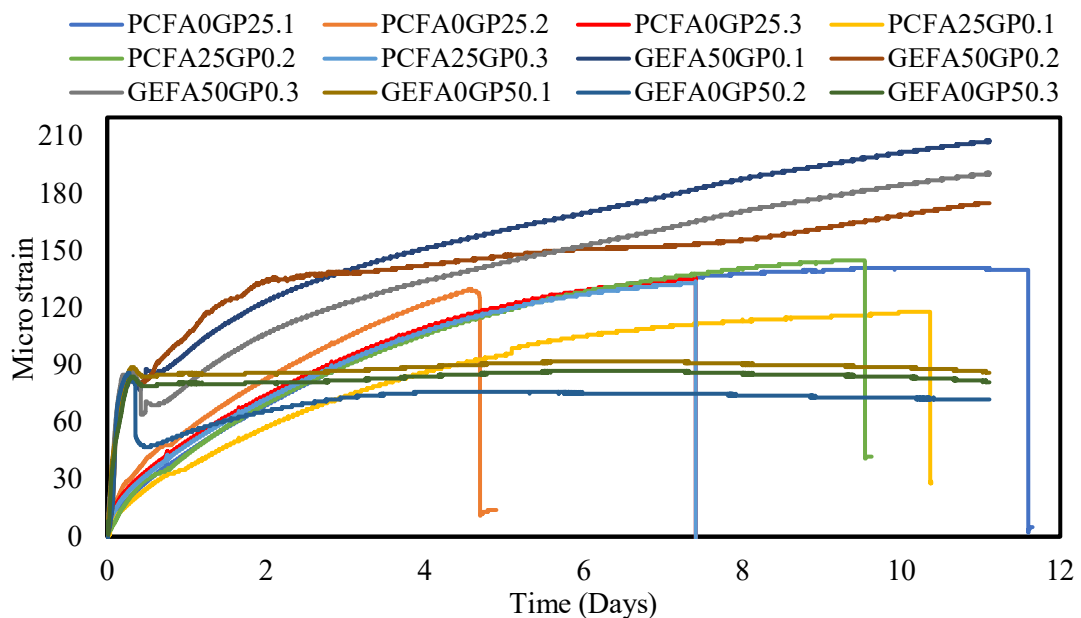


Figure 12. The recorded micro strain values of various mixes.

Figures 13 and 14 provide further information on the cracking style of samples. As can be seen in Figure 13 (a), geopolymer sample produced with fly ash developed a significantly high number of micro cracks on its surface. On the contrary, geopolymer sample produced with 50% glass powder is found to only have large cracks. Although on the top of the geopolymer samples four large cracks can be seen but only two of them had

gone through the body of the samples. Figure 14 provides information on the style of cracks on the body of samples. Based on this figure, cracks produced on geopolymer samples containing glass powder are found to be rather curved, compared to fly ash-based samples. This can be due to higher micro strain values causing the crack propagation to start more from the top in glass powder and connect to the bottom rapidly. Also, it can point to the higher brittleness of mixes produced with glass powder, since glass is also a ceramic material that are known to be more brittle. In addition, the effect of surface adhesion of steel with the samples can have potentially affected the cracking style of samples. Nonetheless in this study, lubricating agents have been applied to the surface of steel ring to ensure minimum adhesion. Figure 15 presents the graphical illustration of cracks produced on specimens, labelled as base mismatch cracks, single-strand cracks, double strand cracks, inter-strand cracks and bulky cracks. Of the mentioned styles outlined, base mismatch cracks are more seen in fly ash containing samples, single-strand break cracks were only seen on top of the geopolymer samples, interstrand crosslinked cracks were seen in portland cement mortars and finally, bulky cracks were only seen in geopolymer samples containing glass powder.



(a): GEFA50GP0



(b): GEFA0GP50

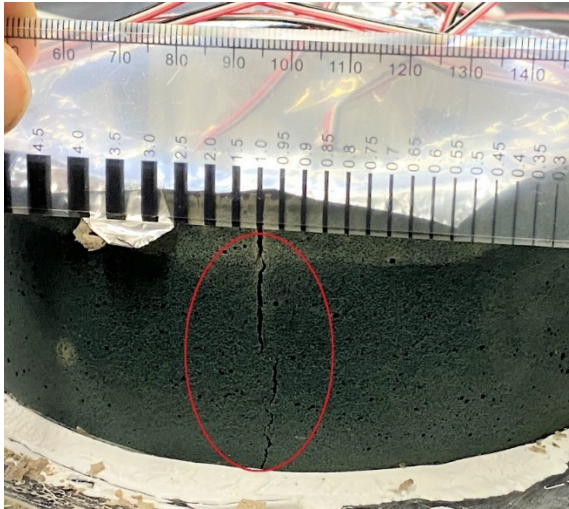


(c): PCFA25GP0

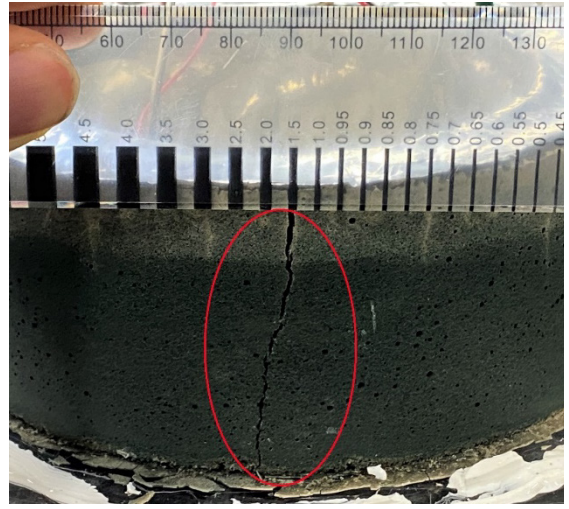


(d): PCFA0GP25

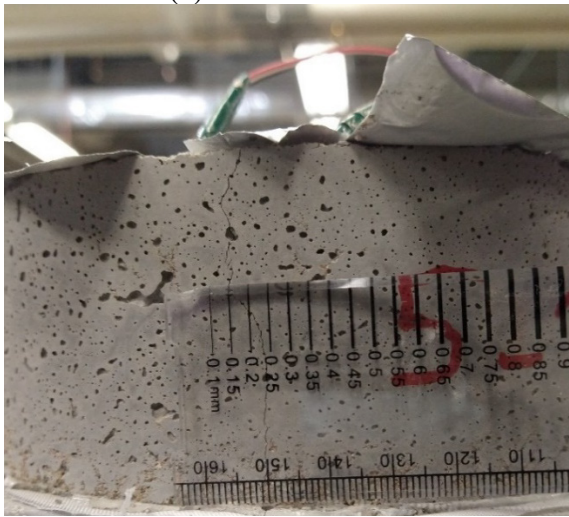
Figure 13. Cracks formed on top of the specimens with (a): GEFA50GP50, (b): GEFA0GP50, (c): PCFA25GP0, (d): PCFA0GP25.



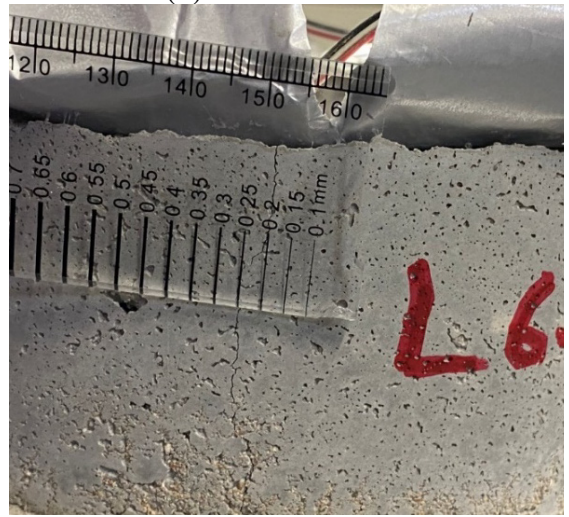
(a): GEFA50GP0



(b): GEFA0GP50



(c): PCFA25GP0



(d): PCFA0GP25

Figure 14. Cracks formed on sides of the specimens with (a): GEFA50GP50, (b): GEFA0GP50, (c): PCFA25GP0, (d): PCFA0GP25.

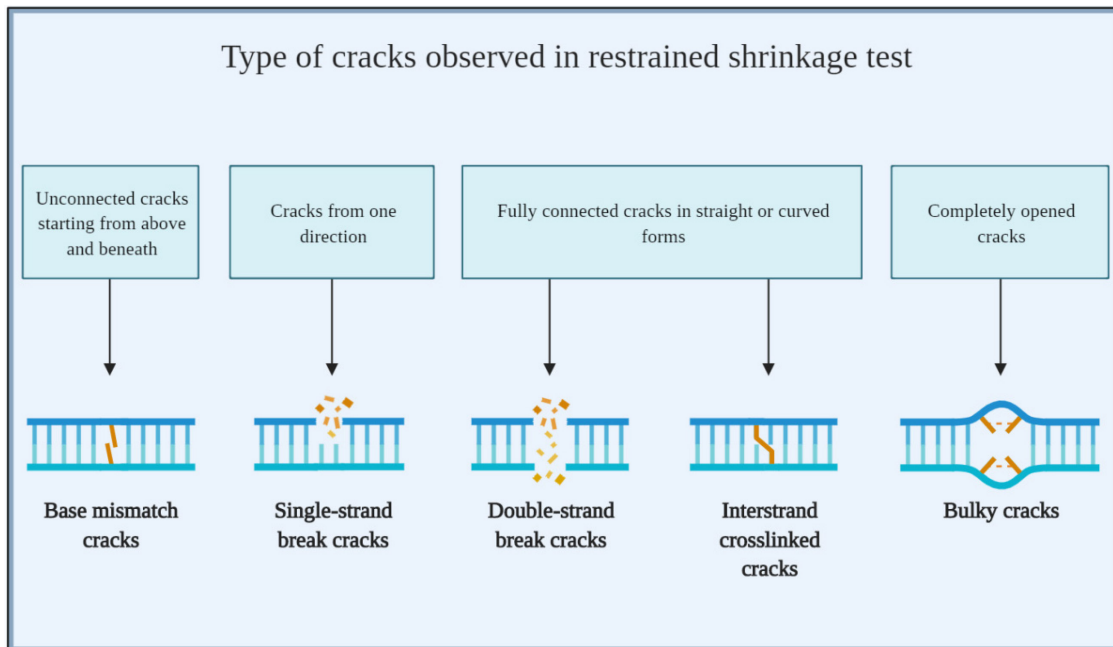


Figure 15. Graphical illustration of the observed cracks.

Table 12. Information about restrained shrinkage specimens.

Sample	Cracking time	Number of full cracks	Max crack size
GEFA50GP0-1	10 h	2	1 mm
GEFA50GP0-2	8.5 h	2	1 mm
GEFA50GP0-3	11 h	2	1.5 mm
Average	9.8 h	2	1.16 mm
GEFA0GP50-1	9 h	2	2 mm
GEFA0GP50-2	10.5 h	2	2 mm
GEFA0GP50-3	11.5 h	2	2 mm
Average	10.3 h	2	2 mm
PCFA25GP0-1	10.4 d	1	0.15 mm
PCFA25GP0-2	9.5 d	1	0.20 mm
PCFA25GP0-3	7.4 d	1	0.25 mm
Average	9.1 d	1	0.20 mm
PCFA0GP25-1	11.6 d	1	0.25 mm
PCFA0GP25-2	4.7 d	1	0.20 mm
PCFA0GP25-3	7.4 d	1	0.20 mm
Average	7.9 d	1	0.21 mm

4.11. Electrical resistivity

Figure 16 presents the result of electrical resistivity measurement after 28 days of curing. Electrical resistivity was conducted to infer permeability and show the potential corrosion tendency of steel bar if the given materials are used for on-site applications.

Based on this figure, geopolymer mixes are found to have considerably lower electrical

resistivity with a mean value of 11.3 $\Omega.m$, compared to 50.8 $\Omega.m$, respectively. This shows a 346% increase in electrical resistivity of mixes produced with portland cement when compared to geopolymer mixes. Further from this figure, the inclusion of glass powder is found to increase the electrical resistivity values in both binding systems. In this regard, the mean $\Omega.m$. values of mixes with and without glass powder is found to be 37 and 25 $\Omega.m.$, respectively. The 45% higher electrical resistivity values can be due to the high resistivity of glass particles. Similarly, Refs. [156], [157] noted that the effect of glass powder on electrical resistivity is directly related to the size of glass particles with finer particles resulting in higher resistivity.

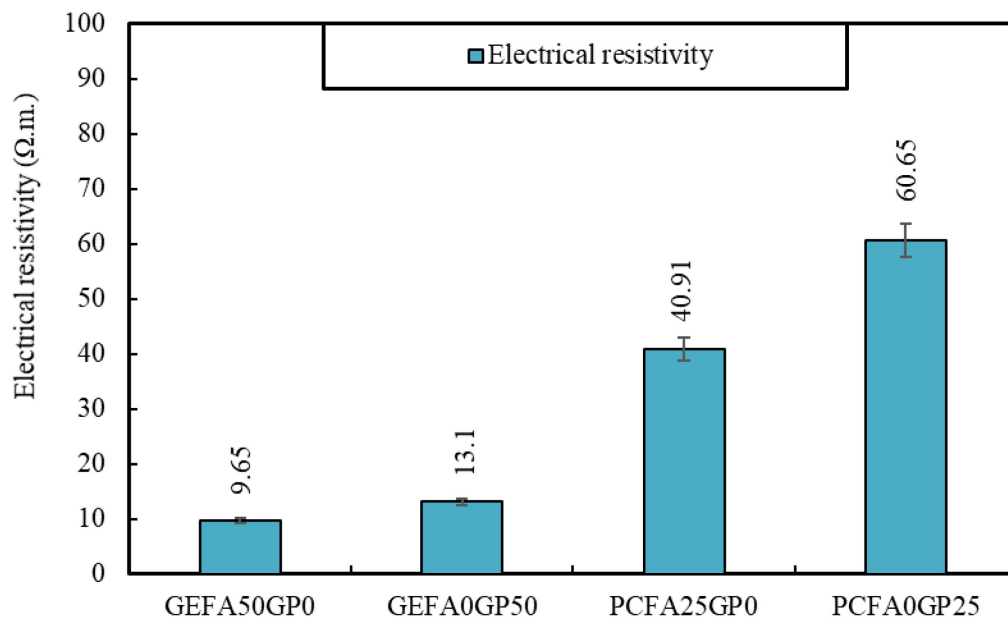


Figure 16. Electrical resistivity of mixes.

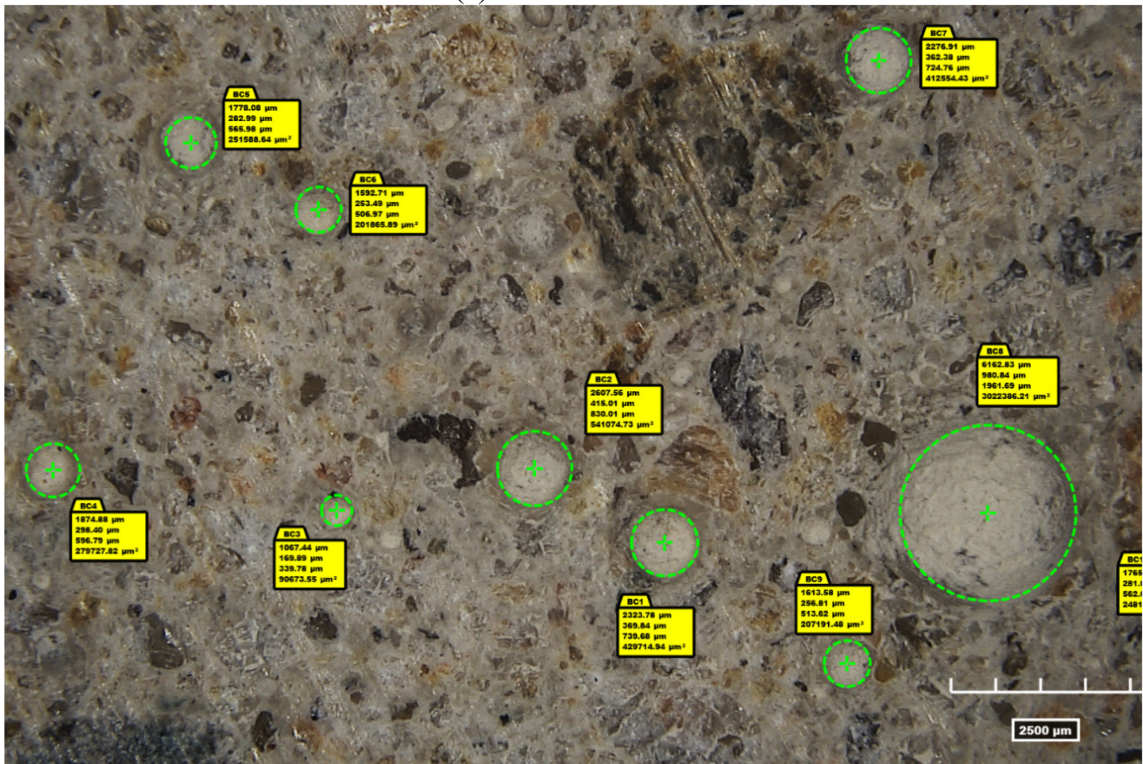
4.12. Surface morphology

To evaluate the surface quality of specimens, Figures 17 (a) through (d) present the digital images of various mixes with size designation of the un-hydrated particles

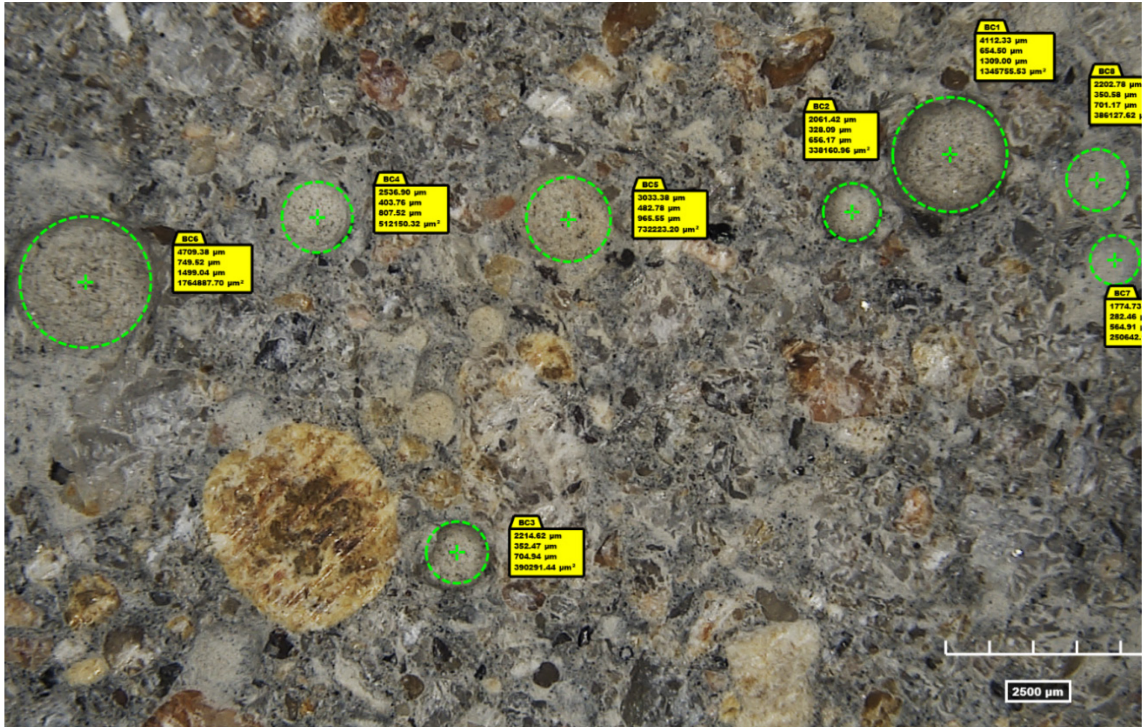
showing length, radius, diameter and area of each circle presented in the yellow boxes. Based on Figure 17 (a) and (b), geopolymer mixes containing glass powder are found to have a higher number of colonies of unreacted particles compared to mixes containing fly ash. Additionally, Figure 17 (c) and (d) present PCFA25GP0 and PCFA0GP25, respectively. The radius, perimeter and areas are also reported in Table 13. Based on these figures and Table 13, portland cement mortar mixes are found to have a generally larger content of unreacted particles which can be due to the lower pH of portland cement mixes, compared to their geopolymer companions [24]. Nonetheless, the content of unreacted fly ash is still lower than the glass powder even in portland cement mortar sample (Figure 17 (c)). The reason for this higher flocculation of glass powder in both binding systems can be the lower particle size diameter of glass powder causing this phenomenon which commonly takes place in nano materials [158]. This can explain the higher water absorption and porosity achieved for mixes containing glass powder in section 4.8. Also, Ref. [151] reported similar colonies of unreacted glass particles and associated it with the glass powder particle size.



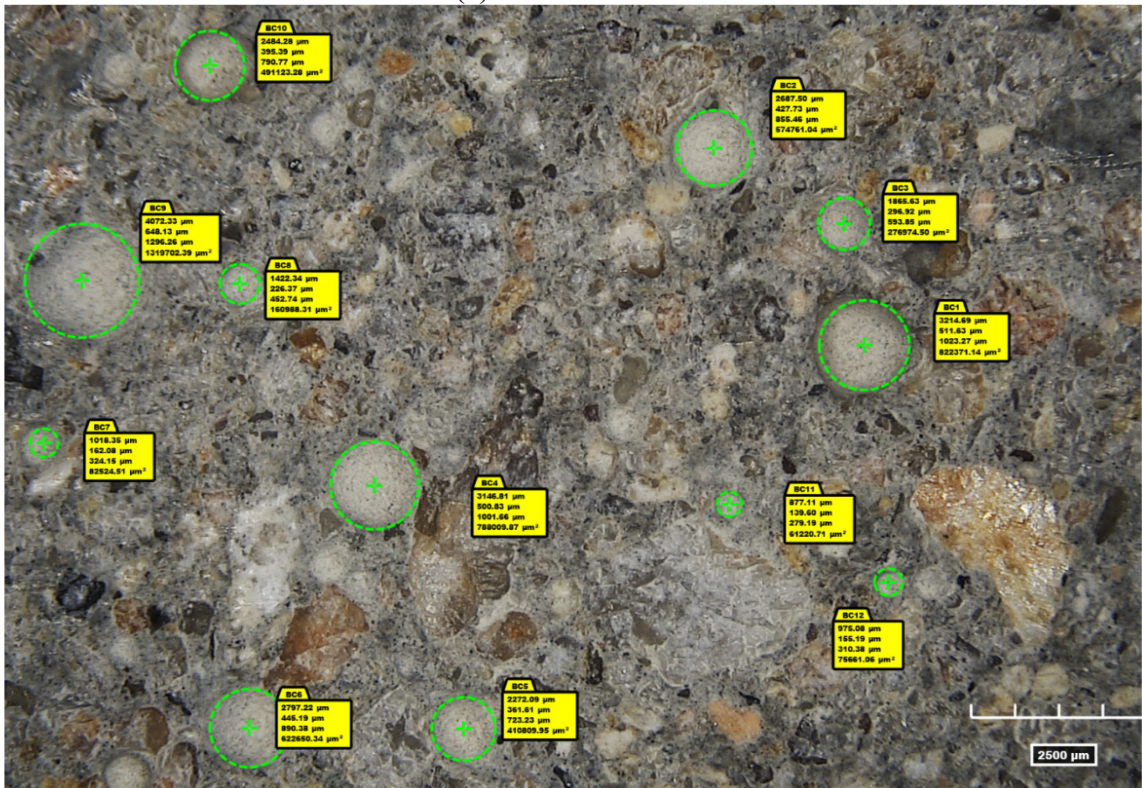
(a): GEFA50GP0



(b): GEFA0GP50



(c): PCFA25GP0



(d): PCFA0GP25

Figure 17. Digital images of mixes with size designation of the un-hydrated particles showing length, radius, diameter and area.

Table 13. Presenting the area and radius of colonies of unreacted particles found in surface morphology test.

Circle ID	Circle perimeter (μm)	Circle radius (μm)	Circle area (μm^2)
GEFA50GP0			
BC1	2482.72	395.14	490507.7
BC2	2303.22	366.57	422144.1
GEFA0GP50			
BC1	2323.78	369.84	429714.9
BC2	2607.56	415.01	541074.7
BC3	1067.44	169.89	90673.55
BC4	1874.88	298.4	279727.8
BC5	1778.08	282.99	251588.6
BC6	1592.71	253.49	201865.9
BC7	2276.91	362.38	412554.4
BC8	6162.83	980.84	3022386
BC9	1613.58	256.81	207191.5
BC10	1765.87	281.05	248146.5
PCFA25GP0			
BC1	4112.33	654.5	1345756
BC2	2061.42	328.09	338161
BC3	2214.62	352.47	390291.4
BC4	2536.9	403.76	512150.3
BC5	3033.38	482.78	732223.2
BC6	4709.38	749.52	1764888
BC7	1774.73	282.46	250642.2
BC8	2202.78	350.58	386127.6
PCFA0GP25			
BC1	3214.69	511.63	822371.1
BC2	2687.5	427.73	574761
BC3	1865.63	296.92	276974.5
BC4	3146.81	500.83	788009.9
BC5	2272.09	361.61	410810
BC6	2797.22	445.19	622650.3
BC7	1018.35	162.08	82524.51
BC8	1422.34	226.37	160988.3
BC9	4072.33	648.13	1319702
BC10	2484.28	395.39	491123.3
BC11	877.11	139.6	61220.71
BC12	975.08	155.19	75661.06

5. CONCLUSION

In this research study, the effect of inclusion of glass powder on the mechanical and cracking properties of portland cement and geopolymer mortars has been evaluated.

Based on the results, the following conclusions can be made:

- Glass powder is an underutilized cementitious material that can be used as a partial replacement of OPC or as a precursor in the production of geopolymer concrete. Its effect on flowability of OPC mixes appeared to be positive in portland cement mixes but in geopolymer mixes it is found to reduce the flowability of fresh mixes. This is further confirmed with the result of air content, fresh and hardened density, as well as electrical resistivity. In all cases, the results are indicative of higher content of pores are produced in specimens that contain glass powder, despite the ultra-fineness of glass powder used in this study.
- The compressive strength values of portland cement mixes containing 25% glass powder are found to be positively affected. However, when substituted 50% fly ash (class F) with glass powder in geopolymer mixes, a slightly lower strength values are achieved. Similar results are found for elastic modulus and splitting tensile strength tests, which point to lower hydration rate of the ultra-fine glass used in geopolymer mixes in this study. The better performance of mixes containing glass powder in portland cement mortars can be due to its better pozzolanic compatibility with the hydraulic reaction of portland cement, compared with geopolymerization process.

- The result of shrinkage tests shows that geopolymer mixes have a significantly higher shrinkage values compared to portland cement mortars. Notably, the incorporation of glass powder is further seen to increase this trend not only in geopolymer mortars but also in their portland cement mortar companions. Similar findings have been documented for restrained shrinkage test conducted in this study with mixes containing glass powder resulted in higher crack width. Additionally, a considerably different type of cracking is seen between the two binders that when glass powder is included, and specimens are found to crack slightly faster than the ones produced with fly ash (class F) in portland cement mortars. Yet, in geopolymer mixes, rather similar to slightly elongated crack propagation is seen. In both binding systems, however, the impact of surface adhesion of mortar with steel ring can be an effective factor. Further studies in this area can potentially focus more on this bonding and its respective impact on cracking. It is worth noting that in geopolymer samples, the cracking of fly ash leans more toward starting from top and the bottom for the two remain unconnected for a longer period of time. For geopolymer samples produced with glass powder, however, the larger cracking width significant affects this and produces a more linear crack in form of double-strand break and bulky cracks as opposed to curved cracks (inter-strand crosslinked cracks) for portland cement mortars. In addition, single strand break cracks have also been observed on the surface of geopolymer mixes containing both glass powder and fly ash.

- The result of the electrical resistivity and abrasion resistance of mixes shows that the inclusion of glass powder performs better than coal fly ash in terms of durability. This is caused by the denser microstructure and hardness of the glass powder used when compared to its companion coal fly ash (class F).
- Images taken with digital microscope have also revealed that the content of unreacted particles are relatively higher in portland cement mortar mixes, compared to geopolymer mixes. The reason for this is hypothesized to be due to the lower pH of portland cement mortar, since the mixing process for all mixtures followed a similar fashion. Nonetheless, mixes produced with glass powder, in either binding system, are also found to have higher content of flocculated and unreacted particles. This can be the reason for higher water absorption and apparent porosity results. The reason for this is believed to be the ultra-fineness of the glass particles causing difficulty in dispersion of materials. Further studies in this area can provide further information on the dispersion properties of ultra-fine glass particles.

Although a comprehensive series of tests conducted in this study, only aluminosilicate glass with a fineness of 6 μm has been used, which can be the limitation of this study. However, the result of this study is found to be significant and point to the potential use of glass powder as a substitute for coal fly ash with major physico-mechanical benefits. Nonetheless, it is recommendable that if the structural use of mixes is relatively restricted, the use of fibers and shrinkage reducing agent can be a mean to address the high cracking tendency of geopolymer concretes.

REFERENCES

- [1] A. International, “ASTM C136-01, Standard Test Method for Sieve Analysis of Fine and Coarse Aggregates,” *ASTM Int. West Conshohocken, PA*, vol. i, no. 200, pp. 1–5, 2001, doi: 10.1520/C0136-01.
- [2] J. Lehne and F. Preston, “Making Concrete Change Innovation in Low-carbon Cement and Concrete The Royal Institute of International Affairs, Chatham House Report Series, [www.chathamhouse.org/sites/default/files/publications/research/2018-06-13-makingconcrete- c](http://www.chathamhouse.org/sites/default/files/publications/research/2018-06-13-makingconcrete-c),” p. 138, 2018, [Online]. Available: www.chathamhouse.org.
- [3] A. Arrigoni *et al.*, “Life cycle greenhouse gas emissions of concrete containing supplementary cementitious materials: cut-off vs. substitution,” *J. Clean. Prod.*, vol. 263, p. 121465, 2020, doi: 10.1016/j.jclepro.2020.121465.
- [4] Statista, “Soft brown coal production top countries 2018 | Statista,” *Statista*, 2020. <https://www-statista-com.ezproxy.sussex.ac.uk/statistics/264779/countries-with-the-largest-soft-brown-coal-production/>.
- [5] B. of L. S. U.S. Department of Labor, “Industries at a Glance: Construction NAICS 23 BLS,” *Bls*, 2020. <https://www.bls.gov/iag/tgs/iag23.htm>.
- [6] A. D. Municipality, “Construction Statistics Report,” vol. 2012, no. October, pp. 1–13, 2011.
- [7] M. Nodehi, A. A. Arani, and V. M. Taghvaei, “Sustainability spillover effects and partnership between East Asia & Pacific versus North America: interactions of social, environment and economy,” *Lett. Spat. Resour. Sci.*, no. 0123456789, 2021, doi: 10.1007/s12076-021-00282-5.

- [8] V. Mohamad Taghvaei *et al.*, “Sustainable development goals: transportation, health and public policy,” *Rev. Econ. Polit. Sci.*, Jan. 2021, doi: 10.1108/REPS-12-2019-0168.
- [9] M. Nodehi and V. M. Taghvaei, “Data and methodology for estimating sustainability spillover effects between two regions,” *Mendeley Data*, 2021, doi: <http://dx.doi.org/10.17632/xvd7bv6mjb.1>.
- [10] V. M. Taghvaei, M. Nodehi, A. A. Arani, Y. Jafari, and J. K. Shirazi, “Sustainability spillover effects of social, environment and economy: mapping global sustainable development in a systematic analysis,” *Asia-Pacific J. Reg. Sci.*, no. 0123456789, 2022, doi: 10.1007/s41685-022-00231-0.
- [11] M. Sandanayake, W. Lokuge, G. Zhang, S. Setunge, and Q. Thushar, “Greenhouse gas emissions during timber and concrete building construction —A scenario based comparative case study,” *Sustain. Cities Soc.*, vol. 38, no. August 2017, pp. 91–97, 2018, doi: 10.1016/j.scs.2017.12.017.
- [12] E. R. Teixeira, R. Mateus, A. F. Camões, L. Bragança, and F. G. Branco, “Comparative environmental life-cycle analysis of concretes using biomass and coal fly ashes as partial cement replacement material,” *J. Clean. Prod.*, vol. 112, pp. 2221–2230, 2016, doi: 10.1016/j.jclepro.2015.09.124.
- [13] O. Gencil *et al.*, “Lightweight foam concrete containing expanded perlite and glass sand: Physico-mechanical, durability, and insulation properties,” *Constr. Build. Mater.*, vol. 320, no. January, p. 126187, Feb. 2022, doi: 10.1016/j.conbuildmat.2021.126187.

- [14] M. Nodehi, T. Ozbakkaloglu, and A. Gholampour, “Effect of supplementary cementitious materials on properties of 3D printed conventional and alkali-activated concrete: A review,” *Autom. Constr.*, vol. 138, p. 104215, Jun. 2022, doi: 10.1016/j.autcon.2022.104215.
- [15] S. A. Miller, “Supplementary cementitious materials to mitigate greenhouse gas emissions from concrete: can there be too much of a good thing?,” *J. Clean. Prod.*, vol. 178, pp. 587–598, 2018, doi: 10.1016/j.jclepro.2018.01.008.
- [16] G. Sauve and K. Van Acker, “The environmental impacts of municipal solid waste landfills in Europe: A life cycle assessment of proper reference cases to support decision making,” *J. Environ. Manage.*, vol. 261, no. August 2019, p. 110216, 2020, doi: 10.1016/j.jenvman.2020.110216.
- [17] M. Nodehi, T. Ozbakkaloglu, A. Gholampour, T. Mohammed, and X. Shi, “The effect of curing regimes on physico-mechanical, microstructural and durability properties of alkali-activated materials: A review,” *Constr. Build. Mater.*, vol. 321, p. 126335, Feb. 2022, doi: 10.1016/j.conbuildmat.2022.126335.
- [18] M. Nodehi, “Epoxy, polyester and vinyl ester based polymer concrete: a review,” *Innov. Infrastruct. Solut.*, vol. 7, no. 1, 2022, doi: 10.1007/s41062-021-00661-3.
- [19] M. Nodehi and V. M. Taghvaei, “Applying Circular Economy to Construction Industry through Use of Waste Materials: A Review of Supplementary Cementitious Materials, Plastics, and Ceramics,” *Circ. Econ. Sustain.*, Jan. 2022, doi: 10.1007/s43615-022-00149-x.

- [20] M. Nodehi and F. Aguayo, "Ultra high performance and high strength geopolymer concrete," *J. Build. Pathol. Rehabil.*, vol. 6, no. 1, p. 34, Dec. 2021, doi: 10.1007/s41024-021-00130-5.
- [21] M. Nodehi and V. Mohamad Taghvaei, "Sustainable concrete for circular economy: a review on use of waste glass," *Glas. Struct. Eng.*, May 2021, doi: 10.1007/s40940-021-00155-9.
- [22] M. Nodehi, "A comparative review on foam-based versus lightweight aggregate-based alkali-activated materials and geopolymer," *Innov. Infrastruct. Solut.*, vol. 6, no. 4, p. 231, Dec. 2021, doi: 10.1007/s41062-021-00595-w.
- [23] J. Li, W. Zhang, C. Li, and P. J. M. Monteiro, "Green concrete containing diatomaceous earth and limestone: Workability, mechanical properties, and life-cycle assessment," *J. Clean. Prod.*, vol. 223, pp. 662–679, 2019, doi: 10.1016/j.jclepro.2019.03.077.
- [24] M. Nodehi and V. M. Taghvaei, "Alkali-Activated Materials and Geopolymer: a Review of Common Precursors and Activators Addressing Circular Economy," *Circ. Econ. Sustain.*, 2021, doi: 10.1007/s43615-021-00029-w.
- [25] H. B. Oakley, "The action of alkalis on clay," *J. Chem. Soc.*, vol. 9, no. 59, pp. 2819–2831, 1927, doi: 10.1039/jr9270002819.
- [26] Z. T. Yao *et al.*, "A comprehensive review on the applications of coal fly ash," *Earth-Science Rev.*, vol. 141, pp. 105–121, 2015, doi: 10.1016/j.earscirev.2014.11.016.

- [27] D. J. M. Flower and J. G. Sanjayan, “Green house gas emissions due to concrete manufacture,” *Int. J. Life Cycle Assess.*, vol. 12, no. 5, pp. 282–288, 2007, doi: 10.1007/s11367-007-0327-3.
- [28] I. Netinger Grubeša, I. Barišic, A. Fucic, and S. S. Bansode, *Characteristics and uses of steel slag in building construction*. 2016.
- [29] Z. Giergiczny, “Fly ash and slag,” *Cem. Concr. Res.*, vol. 124, no. February, 2019, doi: 10.1016/j.cemconres.2019.105826.
- [30] K. L. Scrivener, V. M. John, and E. M. Gartner, “Eco-efficient cements: Potential economically viable solutions for a low-CO₂ cement-based materials industry,” *Cem. Concr. Res.*, vol. 114, no. June, pp. 2–26, 2018, doi: 10.1016/j.cemconres.2018.03.015.
- [31] EIA, “Electricity generation from natural gas and renewables increases as a result of lower natural gas prices and declining costs of solar and wind renewable capacity, making these fuels increasingly competitive,” 2020.
- [32] USEIA, “Nuclear power and the environment - U.S. Energy Information Administration (EIA),” *US. Energy Information Administration*, 2020. <https://www.eia.gov/energyexplained/nuclear/nuclear-power-and-the-environment.php> (accessed Apr. 13, 2021).
- [33] I. B. Topçu and M. Canbaz, “Properties of concrete containing waste glass,” *Cem. Concr. Res.*, vol. 34, no. 2, pp. 267–274, 2004, doi: 10.1016/j.cemconres.2003.07.003.

- [34] A. Omran and A. Tagnit-Hamou, "Performance of glass-powder concrete in field applications," *Constr. Build. Mater.*, vol. 109, pp. 84–95, 2016, doi: 10.1016/j.conbuildmat.2016.02.006.
- [35] Environmental protection agency, "EPA - Glass," 2017. .
- [36] A. Schmitz, J. Kamiński, B. Maria Scalet, and A. Soria, "Energy consumption and CO₂ emissions of the European glass industry," *Energy Policy*, vol. 39, no. 1, pp. 142–155, 2011, doi: 10.1016/j.enpol.2010.09.022.
- [37] O. M. Olofinnade, A. N. Ede, J. M. Ndambuki, B. U. Ngene, I. I. Akinwumi, and O. Ofuyatan, "Strength and microstructure of eco-concrete produced using waste glass as partial and complete replacement for sand," *Cogent Eng.*, vol. 5, no. 1, pp. 1–19, 2018, doi: 10.1080/23311916.2018.1483860.
- [38] S. Ng., "High Costs Put Cracks in Glass-Recycling Programs - WSJ," *Wall street journal*. <https://www.wsj.com/articles/high-costs-put-cracks-in-glass-recycling-programs-1429695003> (accessed Apr. 08, 2021).
- [39] E. L. Tucker, C. C. Ferraro, S. J. Laux, and T. G. Townsend, "Economic and life cycle assessment of recycling municipal glass as a pozzolan in portland cement concrete production," *Resour. Conserv. Recycl.*, vol. 129, no. October 2017, pp. 240–247, 2018, doi: 10.1016/j.resconrec.2017.10.025.
- [40] M. Jiang, X. Chen, F. Rajabipour, and C. T. Hendrickson, "Comparative Life Cycle Assessment of Conventional, Glass Powder, and Alkali-Activated Slag Concrete and Mortar," *J. Infrastruct. Syst.*, vol. 20, no. 4, p. 04014020, 2014, doi: 10.1061/(asce)is.1943-555x.0000211.

- [41] A. Gholampour, V. D. Ho, and T. Ozbakkaloglu, “Ambient-cured geopolymer mortars prepared with waste-based sands: Mechanical and durability-related properties and microstructure,” *Compos. Part B Eng.*, vol. 160, no. July 2018, pp. 519–534, 2019, doi: 10.1016/j.compositesb.2018.12.057.
- [42] D. Mostofinejad, S. M. Hosseini, F. Nosouhian, T. Ozbakkaloglu, and B. Nader Tehrani, “Durability of concrete containing recycled concrete coarse and fine aggregates and milled waste glass in magnesium sulfate environment,” *J. Build. Eng.*, vol. 29, p. 101182, May 2020, doi: 10.1016/j.jobbe.2020.101182.
- [43] A. Gholampour, T. Ozbakkaloglu, and T. D. Ngo, “Development of a waste-based eco-friendly structural mortar without Portland cement and natural sand,” *Struct. Concr.*, vol. 22, no. S1, Jan. 2021, doi: 10.1002/suco.202000096.
- [44] K. Afshinnia and P. R. Rangaraju, “Influence of fineness of ground recycled glass on mitigation of alkali-silica reaction in mortars,” *Constr. Build. Mater.*, vol. 81, pp. 257–267, 2015, doi: 10.1016/j.conbuildmat.2015.02.041.
- [45] A. Sacconi and M. C. Bignozzi, “ASR expansion behavior of recycled glass fine aggregates in concrete,” *Cem. Concr. Res.*, vol. 40, no. 4, pp. 531–536, 2010, doi: 10.1016/j.cemconres.2009.09.003.
- [46] Y. Jani and W. Hogland, “Waste glass in the production of cement and concrete - A review,” *J. Environ. Chem. Eng.*, vol. 2, no. 3, pp. 1767–1775, 2014, doi: 10.1016/j.jece.2014.03.016.
- [47] Y. Liu, C. Shi, Z. Zhang, and N. Li, “An overview on the reuse of waste glasses in alkali-activated materials,” *Resour. Conserv. Recycl.*, vol. 144, no. December 2018, pp. 297–309, 2019, doi: 10.1016/j.resconrec.2019.02.007.

- [48] K. Gorospe, E. Booya, H. Ghaednia, and S. Das, “Effect of various glass aggregates on the shrinkage and expansion of cement mortar,” *Constr. Build. Mater.*, vol. 210, pp. 301–311, 2019, doi: 10.1016/j.conbuildmat.2019.03.192.
- [49] H. Du and K. H. Tan, “Transport properties of concrete with glass powder as supplementary cementitious material,” *ACI Mater. J.*, vol. 112, no. 3, pp. 429–437, 2015, doi: 10.14359/51687363.
- [50] H. Lee, A. Hanif, M. Usman, J. Sim, and H. Oh, “Performance evaluation of concrete incorporating glass powder and glass sludge wastes as supplementary cementing material,” *J. Clean. Prod.*, vol. 170, pp. 683–693, 2018, doi: 10.1016/j.jclepro.2017.09.133.
- [51] N. Schwarz, H. Cam, and N. Neithalath, “Influence of a fine glass powder on the durability characteristics of concrete and its comparison to fly ash,” *Cem. Concr. Compos.*, vol. 30, no. 6, pp. 486–496, 2008, doi: 10.1016/j.cemconcomp.2008.02.001.
- [52] K. L. Jain, G. Sancheti, and L. K. Gupta, “Durability performance of waste granite and glass powder added concrete,” *Constr. Build. Mater.*, vol. 252, p. 119075, 2020, doi: 10.1016/j.conbuildmat.2020.119075.
- [53] H. A. Elaqla, M. A. A. Haloub, and R. N. Rustom, “Effect of new mixing method of glass powder as cement replacement on mechanical behavior of concrete,” *Constr. Build. Mater.*, vol. 203, pp. 75–82, 2019, doi: 10.1016/j.conbuildmat.2019.01.077.

- [54] H. Du and K. H. Tan, "Properties of high volume glass powder concrete," *Cem. Concr. Compos.*, vol. 75, pp. 22–29, 2017, doi: 10.1016/j.cemconcomp.2016.10.010.
- [55] A. A. Aliabdo, A. E. M. Abd Elmoaty, and A. Y. Aboshama, "Utilization of waste glass powder in the production of cement and concrete," *Constr. Build. Mater.*, vol. 124, pp. 866–877, 2016, doi: 10.1016/j.conbuildmat.2016.08.016.
- [56] M. Kamali and A. Ghahremaninezhad, "An investigation into the hydration and microstructure of cement pastes modified with glass powders," *Constr. Build. Mater.*, vol. 112, pp. 915–924, 2016, doi: 10.1016/j.conbuildmat.2016.02.085.
- [57] M. Mirzahosseini and K. A. Riding, "Effect of curing temperature and glass type on the pozzolanic reactivity of glass powder," *Cem. Concr. Res.*, vol. 58, pp. 103–111, 2014, doi: 10.1016/j.cemconres.2014.01.015.
- [58] M. Ohno and V. C. Li, "A feasibility study of strain hardening fiber reinforced fly ash-based geopolymer composites," *Constr. Build. Mater.*, vol. 57, pp. 163–168, 2014, doi: 10.1016/j.conbuildmat.2014.02.005.
- [59] A. Natali, S. Manzi, and M. C. Bignozzi, "Novel fiber-reinforced composite materials based on sustainable geopolymer matrix," *Procedia Eng.*, vol. 21, pp. 1124–1131, 2011, doi: 10.1016/j.proeng.2011.11.2120.
- [60] C. Kuenzel, L. M. Grover, L. Vandeperre, A. R. Boccaccini, and C. R. Cheeseman, "Production of nepheline/quartz ceramics from geopolymer mortars," *J. Eur. Ceram. Soc.*, vol. 33, no. 2, pp. 251–258, 2013, doi: 10.1016/j.jeurceramsoc.2012.08.022.

- [61] Y. M. Liew *et al.*, “Formation of one-part-mixing geopolymers and geopolymer ceramics from geopolymer powder,” *Constr. Build. Mater.*, vol. 156, pp. 9–18, 2017, doi: 10.1016/j.conbuildmat.2017.08.110.
- [62] S. A. Bernal, J. Bejarano, C. Garzón, R. Mejía De Gutiérrez, S. Delvasto, and E. D. Rodríguez, “Performance of refractory aluminosilicate particle/fiber-reinforced geopolymer composites,” *Compos. Part B Eng.*, vol. 43, no. 4, pp. 1919–1928, 2012, doi: 10.1016/j.compositesb.2012.02.027.
- [63] D. M. A. Huiskes, A. Keulen, Q. L. Yu, and H. J. H. Brouwers, “Design and performance evaluation of ultra-lightweight geopolymer concrete,” *Mater. Des.*, vol. 89, pp. 516–526, 2016, doi: 10.1016/j.matdes.2015.09.167.
- [64] P. Posi *et al.*, “Lightweight geopolymer concrete containing aggregate from recycle lightweight block,” *Mater. Des.*, vol. 52, pp. 580–586, 2013, doi: 10.1016/j.matdes.2013.06.001.
- [65] C. R. Shearer, J. L. Provis, S. A. Bernal, and K. E. Kurtis, “Alkali-activation potential of biomass-coal co-fired fly ash,” *Cem. Concr. Compos.*, vol. 73, pp. 62–74, 2016, doi: 10.1016/j.cemconcomp.2016.06.014.
- [66] J. Shekhovtsova, I. Zhernovsky, M. Kovtun, N. Kozhukhova, I. Zhernovskaya, and E. Kearsley, “Estimation of fly ash reactivity for use in alkali-activated cements - A step towards sustainable building material and waste utilization,” *J. Clean. Prod.*, vol. 178, pp. 22–33, 2018, doi: 10.1016/j.jclepro.2017.12.270.
- [67] H. A. Abdel-Gawwad, S. R. V. García, and H. S. Hassan, “Thermal activation of air cooled slag to create one-part alkali activated cement,” *Ceram. Int.*, vol. 44, no. 12, pp. 14935–14939, 2018, doi: 10.1016/j.ceramint.2018.05.089.

- [68] E. Adesanya, K. Ohenoja, T. Luukkonen, P. Kinnunen, and M. Illikainen, “One-part geopolymer cement from slag and pretreated paper sludge,” *J. Clean. Prod.*, vol. 185, pp. 168–175, 2018, doi: 10.1016/j.jclepro.2018.03.007.
- [69] H. Alanazi, M. Yang, D. Zhang, and Z. Gao, “Bond strength of PCC pavement repairs using metakaolin-based geopolymer mortar,” *Cem. Concr. Compos.*, vol. 65, pp. 75–82, 2016, doi: 10.1016/j.cemconcomp.2015.10.009.
- [70] P. Sturm, G. J. G. Gluth, H. J. H. Brouwers, and H. C. Kühne, “Synthesizing one-part geopolymers from rice husk ash,” *Constr. Build. Mater.*, vol. 124, pp. 961–966, 2016, doi: 10.1016/j.conbuildmat.2016.08.017.
- [71] X. Ke, S. A. Bernal, N. Ye, J. L. Provis, and J. Yang, “One-part geopolymers based on thermally treated red Mud/NaOH blends,” *J. Am. Ceram. Soc.*, vol. 98, no. 1, pp. 5–11, 2015, doi: 10.1111/jace.13231.
- [72] N. Ye *et al.*, “Synthesis and strength optimization of one-part geopolymer based on red mud,” *Constr. Build. Mater.*, vol. 111, pp. 317–325, 2016, doi: 10.1016/j.conbuildmat.2016.02.099.
- [73] M. X. Peng *et al.*, “Effects of alkali on one-part alkali-activated cement synthesized by calcining bentonite with dolomite and Na₂CO₃,” *Appl. Clay Sci.*, vol. 139, pp. 64–71, 2017, doi: 10.1016/j.clay.2017.01.020.
- [74] A. Hajimohammadi and J. S. J. van Deventer, “Characterisation of One-Part Geopolymer Binders Made from Fly Ash,” *Waste and Biomass Valorization*, vol. 8, no. 1, pp. 225–233, 2017, doi: 10.1007/s12649-016-9582-5.

- [75] H. Tchakoute Kouamo, A. Elimbi, J. A. Mbey, C. J. Ngally Sabouang, and D. Njopwouo, “The effect of adding alumina-oxide to metakaolin and volcanic ash on geopolymer products: A comparative study,” *Constr. Build. Mater.*, vol. 35, pp. 960–969, 2012, doi: 10.1016/j.conbuildmat.2012.04.023.
- [76] EIA, “Electricity and the environment - U.S. Energy Information Administration (EIA),” 2018, 2020. <https://www.eia.gov/energyexplained/electricity/electricity-and-the-environment.php> (accessed Jan. 05, 2020).
- [77] Y. Gao, B. He, Y. Li, J. Tang, and L. Qu, “Effects of nano-particles on improvement in wear resistance and drying shrinkage of road fly ash concrete,” *Constr. Build. Mater.*, vol. 151, pp. 228–235, 2017, doi: 10.1016/j.conbuildmat.2017.06.080.
- [78] B. Lu *et al.*, “Designing spray-based 3D printable cementitious materials with fly ash cenosphere and air entraining agent,” *Constr. Build. Mater.*, vol. 211, pp. 1073–1084, 2019, doi: 10.1016/j.conbuildmat.2019.03.186.
- [79] B. Panda, S. Ruan, C. Unluer, and M. J. Tan, “Improving the 3D printability of high volume fly ash mixtures via the use of nano attapulgite clay,” *Compos. Part B Eng.*, vol. 165, no. June 2018, pp. 75–83, 2019, doi: 10.1016/j.compositesb.2018.11.109.
- [80] P. min Zhan *et al.*, “Utilization of nano-metakaolin in concrete: A review,” *J. Build. Eng.*, vol. 30, no. October 2019, p. 101259, 2020, doi: 10.1016/j.job.2020.101259.
- [81] J. Xie *et al.*, “Effect of nano metakaolin on compressive strength of recycled concrete,” *Constr. Build. Mater.*, vol. 256, 2020, doi: 10.1016/j.conbuildmat.2020.119393.

- [82] R. Muduli and B. B. Mukharjee, “Performance assessment of concrete incorporating recycled coarse aggregates and metakaolin: A systematic approach,” *Constr. Build. Mater.*, vol. 233, p. 117223, 2020, doi: 10.1016/j.conbuildmat.2019.117223.
- [83] N. Tebbal and Z. El Abidine Rahmouni, “Rheological and Mechanical Behavior of Mortars with Metakaolin Formulation,” *Procedia Comput. Sci.*, vol. 158, pp. 45–50, 2019, doi: 10.1016/j.procs.2019.09.026.
- [84] V. Nežerka, P. Bílý, V. Hrbek, and J. Fládr, “Impact of silica fume, fly ash, and metakaolin on the thickness and strength of the ITZ in concrete,” *Cem. Concr. Compos.*, vol. 103, no. January, pp. 252–262, 2019, doi: 10.1016/j.cemconcomp.2019.05.012.
- [85] M. Tyrer, *Municipal solid waste incinerator (MSWI) concrete*. 2013.
- [86] F. Agrela, M. Cabrera, M. M. Morales, M. Zamorano, and M. Alshaaer, *Biomass fly ash and biomass bottom ash*, vol. 3. 2018.
- [87] S. Wang and L. Baxter, “Comprehensive study of biomass fly ash in concrete: Strength, microscopy, kinetics and durability,” *Fuel Process. Technol.*, vol. 88, no. 11–12, pp. 1165–1170, 2007, doi: 10.1016/j.fuproc.2007.06.016.
- [88] C. Shi, “Steel Slag—Its Production, Processing, Characteristics, and Cementitious Properties,” *J. Mater. Civ. Eng.*, vol. 16, no. 3, pp. 230–236, 2004, doi: 10.1061/(asce)0899-1561(2004)16:3(230).
- [89] H. Qasrawi, F. Shalabi, and I. Asi, “Use of low CaO unprocessed steel slag in concrete as fine aggregate,” *Constr. Build. Mater.*, vol. 23, no. 2, pp. 1118–1125, 2009, doi: 10.1016/j.conbuildmat.2008.06.003.

- [90] V. Subathra Devi and B. K. Gnanavel, “Properties of concrete manufactured using steel slag,” *Procedia Eng.*, vol. 97, pp. 95–104, 2014, doi: 10.1016/j.proeng.2014.12.229.
- [91] S. Sun *et al.*, “Geopolymer synthesized from sludge residue pretreated by the wet alkalinizing method: Compressive strength and immobilization efficiency of heavy metal,” *Constr. Build. Mater.*, vol. 170, pp. 619–626, 2018, doi: 10.1016/j.conbuildmat.2018.03.068.
- [92] S. Yan and K. Sagoe-Crentsil, “Properties of wastepaper sludge in geopolymer mortars for masonry applications,” *J. Environ. Manage.*, vol. 112, pp. 27–32, 2012, doi: 10.1016/j.jenvman.2012.07.008.
- [93] R. Obenaus-Emler, M. Falah, and M. Illikainen, “Assessment of mine tailings as precursors for alkali-activated materials for on-site applications,” *Constr. Build. Mater.*, vol. 246, p. 118470, 2020, doi: 10.1016/j.conbuildmat.2020.118470.
- [94] Z. Xiaolong, Z. Shiyu, L. Hui, and Z. Yingliang, “Disposal of mine tailings via geopolymerization,” *J. Clean. Prod.*, vol. 284, no. xxxx, p. 124756, 2021, doi: 10.1016/j.jclepro.2020.124756.
- [95] R. Si, S. Guo, Q. Dai, and J. Wang, “Atomic-structure, microstructure and mechanical properties of glass powder modified metakaolin-based geopolymer,” *Constr. Build. Mater.*, vol. 254, p. 119303, 2020, doi: 10.1016/j.conbuildmat.2020.119303.
- [96] R. Si, Q. Dai, S. Guo, and J. Wang, “Mechanical property, nanopore structure and drying shrinkage of metakaolin-based geopolymer with waste glass powder,” *J. Clean. Prod.*, vol. 242, p. 118502, 2020, doi: 10.1016/j.jclepro.2019.118502.

- [97] A. Khmiri, M. Chaabouni, and B. Samet, “Chemical behaviour of ground waste glass when used as partial cement replacement in mortars,” *Constr. Build. Mater.*, vol. 44, pp. 74–80, 2013, doi: 10.1016/j.conbuildmat.2013.02.040.
- [98] Y. Maltais and J. Marchand, “Influence of curing temperature on cement hydration and mechanical strength development of fly ash mortars,” *Cem. Concr. Res.*, vol. 27, no. 7, pp. 1009–1020, 1997, doi: 10.1016/S0008-8846(97)00098-7.
- [99] R. Idir, M. Cyr, and A. Pavoine, “Investigations on the durability of alkali-activated recycled glass,” *Constr. Build. Mater.*, vol. 236, p. 117477, 2020, doi: 10.1016/j.conbuildmat.2019.117477.
- [100] K. Pimraksa, P. Chindaprasirt, A. Rungchet, K. Sagoe-Crentsil, and T. Sato, “Lightweight geopolymer made of highly porous siliceous materials with various Na₂O/Al₂O₃ and SiO₂/Al₂O₃ ratios,” *Mater. Sci. Eng. A*, vol. 528, no. 21, pp. 6616–6623, 2011, doi: 10.1016/j.msea.2011.04.044.
- [101] C. Tippayasam *et al.*, “Potassium alkali concentration and heat treatment affected metakaolin-based geopolymer,” *Constr. Build. Mater.*, vol. 104, pp. 293–297, 2016, doi: 10.1016/j.conbuildmat.2015.11.027.
- [102] NIOSH, “Sodium Hydroxide | NIOSH | CDC.” .
- [103] P. Giannaros, A. Kanellopoulos, and A. Al-Tabbaa, “Sealing of cracks in cement using microencapsulated sodium silicate,” *Smart Mater. Struct.*, vol. 25, no. 8, 2016, doi: 10.1088/0964-1726/25/8/084005.
- [104] C. T. Miller, *Groundwater Quality.*, vol. 59, no. 6. 1987.
- [105] M. B. Hocking, “Industrial Bases by Chemical Routes,” *Handb. Chem. Technol. Pollut. Control*, pp. 201–220, 2005, doi: 10.1016/b978-012088796-5/50010-7.

- [106] J. G. Speight, *Industrial Inorganic Chemistry*, no. Chapter 2. 2017.
- [107] K. E. Haneke, “Sodium Metasilicate Pentahydrate [10213-79-3], and Sodium Metasilicate Nonahydrate [13517-24-3] Review of Toxicological Literature Sodium Metasilicate , Anhydrous [6834-92-0], Sodium Metasilicate Pentahydrate [10213-79-3], and Sodium Metasilicate,” no. January, 2002.
- [108] Encyclopedia.com, “Potassium Hydroxide | Encyclopedia.com,” 2020. <https://www.encyclopedia.com/science/academic-and-educational-journals/potassium-hydroxide> (accessed Apr. 21, 2021).
- [109] S. K. Nath and S. Kumar, “Role of alkali concentration on reaction kinetics of fly ash geopolymerization,” *J. Non. Cryst. Solids*, vol. 505, no. September 2018, pp. 241–251, 2019, doi: 10.1016/j.jnoncrysol.2018.11.007.
- [110] G. Görhan and G. Kürklü, “The influence of the NaOH solution on the properties of the fly ash-based geopolymer mortar cured at different temperatures,” *Compos. Part B Eng.*, vol. 58, pp. 371–377, 2014, doi: 10.1016/j.compositesb.2013.10.082.
- [111] H. Xu and J. S. J. Van Deventer, “The geopolymerisation of alumino-silicate minerals,” *Int. J. Miner. Process.*, vol. 59, no. 3, pp. 247–266, 2000, doi: 10.1016/S0301-7516(99)00074-5.
- [112] A. D. Hounsi *et al.*, “How does Na, K alkali metal concentration change the early age structural characteristic of kaolin-based geopolymers,” *Ceram. Int.*, vol. 40, no. 7 PART A, pp. 8953–8962, 2014, doi: 10.1016/j.ceramint.2014.02.052.
- [113] S. B. Park, B. C. Lee, and J. H. Kim, “Studies on mechanical properties of concrete containing waste glass aggregate,” *Cem. Concr. Res.*, vol. 34, no. 12, pp. 2181–2189, 2004, doi: 10.1016/j.cemconres.2004.02.006.

- [114] X. Yu, Z. Tao, T. Y. Song, and Z. Pan, “Performance of concrete made with steel slag and waste glass,” *Constr. Build. Mater.*, vol. 114, pp. 737–746, 2016, doi: 10.1016/j.conbuildmat.2016.03.217.
- [115] T. Tho-In, V. Sata, K. Boonserm, and P. Chindapasirt, “Compressive strength and microstructure analysis of geopolymer paste using waste glass powder and fly ash,” *J. Clean. Prod.*, vol. 172, pp. 2892–2898, 2016, doi: 10.1016/j.jclepro.2017.11.125.
- [116] I. Khan, T. Xu, A. Castel, R. I. Gilbert, and M. Babae, “Risk of early age cracking in geopolymer concrete due to restrained shrinkage,” *Constr. Build. Mater.*, vol. 229, p. 116840, 2019, doi: 10.1016/j.conbuildmat.2019.116840.
- [117] M. Mastali, P. Kinnunen, A. Dalvand, R. Mohammadi Firouz, and M. Illikainen, “Drying shrinkage in alkali-activated binders – A critical review,” *Constr. Build. Mater.*, vol. 190, pp. 533–550, 2018, doi: 10.1016/j.conbuildmat.2018.09.125.
- [118] D. Ballekere Kumarappa, S. Peethamparan, and M. Ngami, “Autogenous shrinkage of alkali activated slag mortars: Basic mechanisms and mitigation methods,” *Cem. Concr. Res.*, vol. 109, no. July 2017, pp. 1–9, 2018, doi: 10.1016/j.cemconres.2018.04.004.
- [119] W. Rakngan, T. Williamson, R. D. Ferron, G. Sant, and M. C. G. Juenger, “Controlling workability in alkali-activated Class C fly ash,” *Constr. Build. Mater.*, vol. 183, pp. 226–233, 2018, doi: 10.1016/j.conbuildmat.2018.06.174.
- [120] L. Coppola *et al.*, “The combined use of admixtures for shrinkage reduction in one-part alkali activated slag-based mortars and pastes,” *Constr. Build. Mater.*, vol. 248, p. 118682, 2020, doi: 10.1016/j.conbuildmat.2020.118682.

- [121] A. A. Melo Neto, M. A. Cincotto, and W. Repette, “Drying and autogenous shrinkage of pastes and mortars with activated slag cement,” *Cem. Concr. Res.*, vol. 38, no. 4, pp. 565–574, 2008, doi: 10.1016/j.cemconres.2007.11.002.
- [122] Y. Wang, T. Zheng, X. Zheng, Y. Liu, J. Darkwa, and G. Zhou, “Thermo-mechanical and moisture absorption properties of fly ash-based lightweight geopolymer concrete reinforced by polypropylene fibers,” *Constr. Build. Mater.*, vol. 251, p. 118960, 2020, doi: 10.1016/j.conbuildmat.2020.118960.
- [123] M. Lizcano, A. Gonzalez, S. Basu, K. Lozano, and M. Radovic, “Effects of water content and chemical composition on structural properties of alkaline activated metakaolin-based geopolymers,” *J. Am. Ceram. Soc.*, vol. 95, no. 7, pp. 2169–2177, 2012, doi: 10.1111/j.1551-2916.2012.05184.x.
- [124] P. Steins, A. Poulesquen, O. Diat, and F. Frizon, “Structural evolution during geopolymerization from an early age to consolidated material,” *Langmuir*, vol. 28, no. 22, pp. 8502–8510, 2012, doi: 10.1021/la300868v.
- [125] S. Bhowmick, G. Le, and A. Verma, “Edited by Narottam P . Bansal and Prabhakar Singh Copyright © 2011 The American Ceramic Society,” vol. 005, no. 860, pp. 115–124, 2011.
- [126] M. Criado, A. Palomo, and A. Fernández-Jiménez, “Alkali activation of fly ashes. Part 1: Effect of curing conditions on the carbonation of the reaction products,” *Fuel*, vol. 84, no. 16, pp. 2048–2054, 2005, doi: 10.1016/j.fuel.2005.03.030.
- [127] S. Aydin and B. Baradan, “Mechanical and microstructural properties of heat cured alkali-activated slag mortars,” *Mater. Des.*, vol. 35, pp. 374–383, 2012, doi: 10.1016/j.matdes.2011.10.005.

- [128] ASTM C33/C33M, “Standard specification for concrete aggregates,” *ASTM Int.*, 2016, doi: 10.1520/C0033.
- [129] X. Shi, Z. Grasley, J. Hogancamp, L. Brescia-Norambuena, A. Mukhopadhyay, and D. Zollinger, “Microstructural, Mechanical, and Shrinkage Characteristics of Cement Mortar Containing Fine Reclaimed Asphalt Pavement,” *J. Mater. Civ. Eng.*, vol. 32, no. 4, p. 04020050, 2020, doi: 10.1061/(asce)mt.1943-5533.0003110.
- [130] ASTM/C143M-15a, “Standard Test Method for Slump of Hydraulic Cement Concrete (C 143),” *ASTM Int.*, vol. 27, pp. 99–101, 2009, doi: 10.1520/C1437-15.2.
- [131] ASTM C230, “Standard Specification for Flow Table for Use in Tests of Hydraulic Cement 1,” *Annu. B. ASTM Stand.*, pp. 4–9, 2010, doi: 10.1520/C0230.
- [132] Astm:C138/C138M-13, “Standard Test Method for Density (Unit Weight), Yield, and Air Content (Gravimetric),” *ASTM Int.*, vol. i, pp. 23–26, 2013, doi: 10.1520/C0138.
- [133] ASTM C39/C39M, “Standard Test Method for Compressive Strength of Cylindrical Concrete Specimens 1,” *ASTM Stand. B.*, vol. i, no. March, pp. 1–5, 2003, doi: 10.1520/C0039.
- [134] ASTM C469-11, “Standard Test Method for Splitting Tensile Strength of Cylindrical Concrete Specimens,” *Man. Hydrocarb. Anal. 6th Ed.*, vol. i, pp. 545-545–3, 2008, doi: doi.org/10.1520/C0469_C0469M-14.
- [135] ASTM C469, “Standard Test Method for Static Modulus of Elasticity and Poisson’s Ratio of Concrete in Compression,” *ASTM Int.*, vol. i, pp. 1–5, 2014, doi: 10.1520/C0469.

- [136] ASTM, “Standard Test Method for Abrasion Resistance of Concrete or Mortar Surfaces by the Rotating-Cutter Method,” *ASTM (American Soc. Test. Mater.)*, 2012, doi: 10.1520/mnl10913m.
- [137] A. C1760/1876, “ASTM Standard C1760 - Standard Test Method for Bulk Electrical Conductivity of Hardened Concrete,” *ASTM Int.*, vol. i, no. c, pp. 1–5, 2012, doi: 10.1520/C1760-12.2.
- [138] American Society for Testing and Materials, “ASTM C20 - 00(2010) ‘Standard Test Methods for Apparent Porosity, Water Absorption, Apparent Specific Gravity, and Bulk Density of Burned Refractory Brick and Shapes by Boiling Water,’” *Refract. Stand.*, vol. i, no. Reapproved 2015, pp. 1–3, 2010, doi: 10.1520/C0020-00R15.
- [139] ASTM:C157/C157M-08, “Standard Test Method for Length Change of Hardened Hydraulic-Cement Mortar and Concrete,” *ASTM Int.*, vol. 08, no. Reapproved, pp. 1–7, 2008, doi: 10.1520/C0157.
- [140] American Society for Testing and Materials ASTM C 1581, “Standard Test Method for Determining Age at Cracking and Induced Tensile Stress Characteristics of Mortar and Concrete under Restrained Shrinkage,” *ASTM Int.*, pp. 1–7, 2009, doi: 10.1520/C1581.
- [141] S. Pyo, S. Y. Abate, and H. K. Kim, “Abrasion resistance of ultra high performance concrete incorporating coarser aggregate,” *Constr. Build. Mater.*, vol. 165, pp. 11–16, 2018, doi: 10.1016/j.conbuildmat.2018.01.036.

- [142] M. Safiuddin and B. Scott, “Abrasion resistance of concrete–Design, construction and case study,” *Concr. Res. Lett.*, vol. 6, no. September 2015, pp. 136–148, 2015, [Online]. Available: https://www.researchgate.net/profile/Md_Safiuddin/publication/281594259_Abrasion_Resistance_of_Concrete_-_Design_Construction_and_Case_Study/links/57bb3c2308ae8a9fc4c27808/Abrasion-Resistance-of-Concrete-Design-Construction-and-Case-Study.pdf.
- [143] G. Pluvinage, J. Capelle, and C. Schmitt, *Methods for assessing defects leading to gas pipe failure*. Elsevier Ltd., 2016.
- [144] X. Shi, L. Brescia-Norambuena, Z. Grasley, and J. Hogancamp, “Fracture Properties and Restrained Shrinkage Cracking Resistance of Cement Mortar Reinforced by Recycled Steel Fiber from Scrap Tires,” *Transp. Res. Rec.*, vol. 2674, no. 8, pp. 581–590, 2020, doi: 10.1177/0361198120924407.
- [145] P. Alberdi-Pagola, V. Marcos-Meson, and G. Fischer, “Fibre Reinforced Cement Sheaths for Zonal Isolation in Oil Wells – Quantification and Mitigation of Shrinkage-Induced Cracking,” 2022, pp. 727–738.
- [146] M. V. Tran, Y. T. H. Cu, and C. V. H. Le, “Rheology and shrinkage of concrete using polypropylene fiber for 3D concrete printing,” *J. Build. Eng.*, vol. 44, no. October, p. 103400, 2021, doi: 10.1016/j.jobe.2021.103400.
- [147] J. Hogancamp and Z. Grasley, “The use of microfine cement to enhance the efficacy of carbon nanofibers with respect to drying shrinkage crack resistance of portland cement mortars,” *Cem. Concr. Compos.*, vol. 83, pp. 405–414, 2017, doi: 10.1016/j.cemconcomp.2017.08.006.

- [148] ASTM C1202, “Standard Test Method for Electrical Indication of Concrete’s Ability to Resist Chloride Ion Penetration,” *Am. Soc. Test. Mater.*, no. C, pp. 1–8, 2012, doi: 10.1520/C1202-12.2.
- [149] X. Jiang, R. Xiao, Y. Ma, M. Zhang, Y. Bai, and B. Huang, “Influence of waste glass powder on the physico-mechanical properties and microstructures of fly ash-based geopolymer paste after exposure to high temperatures,” *Constr. Build. Mater.*, vol. 262, p. 120579, Nov. 2020, doi: 10.1016/j.conbuildmat.2020.120579.
- [150] N. Schwarz, M. DuBois, and N. Neithalath, “Electrical conductivity based characterization of plain and coarse glass powder modified cement pastes,” *Cem. Concr. Compos.*, vol. 29, no. 9, pp. 656–666, 2007, doi: 10.1016/j.cemconcomp.2007.05.005.
- [151] A. Gholampour, T. Ozbakkaloglu, E. Etemadi, and T. Vincent, “Sustainable mortars containing fly ash, glass powder and blast-furnace and lead-smelter slag,” *Mag. Concr. Res.*, vol. 72, no. 9, pp. 447–459, 2020, doi: 10.1680/jmacr.19.00355.
- [152] S. Ibrahim and A. Meawad, “Towards green concrete: Study the role of waste glass powder on cement/superplasticizer compatibility,” *J. Build. Eng.*, vol. 47, no. November 2021, p. 103751, 2022, doi: 10.1016/j.job.2021.103751.
- [153] Y. Jiang, T.-C. Ling, K. H. Mo, and C. Shi, “A critical review of waste glass powder – Multiple roles of utilization in cement-based materials and construction products,” *J. Environ. Manage.*, vol. 242, pp. 440–449, Jul. 2019, doi: 10.1016/j.jenvman.2019.04.098.
- [154] P. Turgut, “Limestone dust and glass powder wastes as new brick material,” *Mater. Struct.*, vol. 41, no. 5, pp. 805–813, Jun. 2008, doi: 10.1617/s11527-007-9284-3.

- [155] A. Shayan and A. Xu, "Performance of glass powder as a pozzolanic material in concrete: A field trial on concrete slabs," *Cem. Concr. Res.*, vol. 36, no. 3, pp. 457–468, Mar. 2006, doi: 10.1016/j.cemconres.2005.12.012.
- [156] S. Tariq, A. N. Scott, J. R. Mackechnie, and V. Shah, "Durability of high volume glass powder self-compacting concrete," *Appl. Sci.*, vol. 10, no. 22, pp. 1–20, 2020, doi: 10.3390/app10228058.
- [157] H. Du and K. H. Tan, "Waste glass powder as cement replacement in concrete," *J. Adv. Concr. Technol.*, vol. 12, no. 11, pp. 468–477, 2014, doi: 10.3151/jact.12.468.
- [158] J. Kruger, S. Zeranka, and G. van Zijl, "An ab initio approach for thixotropy characterisation of (nanoparticle-infused) 3D printable concrete," *Constr. Build. Mater.*, vol. 224, pp. 372–386, 2019, doi: 10.1016/j.conbuildmat.2019.07.078.